JOURNAL OF GEOPHYSICAL RESEARCH, VOL. 100, NO. D12, PAGES 26,141–26,161, DECEMBER 20, 1995

Three dimensional atmospheric transport simulation of the radioactive tracers ^{210}Pb, ^{7}Be, ^{10}Be, and ^{90}Sr

Stefan Rehfeld and Martin Heimann

Max-Planck-Institut für Meteorologie, Hamburg, Germany

Abstract. A global three-dimensional transport model of the atmosphere, having a grid resolution of 7.83° (latitude) x 10° (longitude) x 19 layers in the vertical and driven by European Centre for Medium Range Weather Forecasts (ECMWF) wind field analyses of 1990, is used to simulate the distribution of natural (^{210}Pb, ^{7}Be, ^{10}Be) and artificial (^{90}Sr), radioactive, water-soluble, aerosol-borne tracers. Because of their well-known source-sink distribution these tracers build an ideal tool to depict transport processes in the whole atmosphere and to test the models ability of reproducing these. In particular, this paper focuses on mass exchange between stratosphere and troposphere, using the concentration ratio ^{10}Be/^{7}Be as an indicator. In general, the agreement between observations and model results is quite good, except in polar regions. Modeled arctic ^{210}Pb and ^{7}Be concentrations are overestimated and the annual cycle is underestimated. The modeled antarctic annual cycle of ^{10}Be/^{7}Be shows maxima in winter and spring, whereas the observations exhibit a summer maximum. These discrepancies are attributed to deficiencies in ECMWF wind fields, to differences between observed and model used precipitation, and to the employed parameterization schemes of dry and wet deposition which may be inadequate in the cold polar regions.

Introduction

Natural and artificial, radioactive, water-soluble, aerosol-borne tracers are an ideal tool to study atmospheric transport processes. The source distribution of these elements is relatively well known; they are removed from the atmosphere only by radioactive decay as well as by dry and wet deposition, and many observations exist to be compared with transport model results. Radioactive tracers in the atmosphere may be divided into three groups [*Junge,* 1963]: (1) natural radioactivity from emissions out of the Earth's surface; (2) natural radioactivity produced by cosmic radiation; and (3) artificial radioactivity introduced by nuclear weapon tests.

We choose from the first group ^{210}Pb, which is a decay product of the water-insoluble inert gas ^{222}Rn, emanating from ice-free land surfaces into the atmosphere. From the second group, ^{7}Be and ^{10}Be are selected. Two thirds of the production of ^{7}Be and ^{10}Be takes place in the stratosphere, one third in the troposphere [*Lal and Peters,* 1967]. ^{90}Sr, selected from the artificial radioactivity group, has a stratospheric input.

The isotopes ^{210}Pb, ^{7}Be, ^{10}Be and ^{90}Sr become quickly attached to aerosols after their formation [*Junge,* 1963]. The radii of these aerosol particles lie between 2×10^{-2} and 1 μm [*Graustein and Turekian,* 1986; *Turekian et al.,* 1977; *Feichter et al.,* 1991; *Junge,* 1963; *Brost et al.,* 1991; *Feely et al.,* 1966]. The atmospheric lifetime of these aerosols, which can be defined as the ratio of atmospheric tracer mass to their deposition rate [*Ehhalt,* 1973], is investigated in this paper.

Because of the source distribution and short lifetime of ^{222}Rn, its long-lived decay product ^{210}Pb is predominantly produced in the continental planetary boundary layer. It allows an investigation of transport and removal processes in the lower troposphere, for example, the monsoon circulation or the transport from midlatitudes into the polar regions [*Lambert et al.,* 1990].

Four processes influence the surface concentration of ^{7}Be [*Feely et al.,* 1988]: wet deposition, mass exchange between stratosphere and troposphere, vertical transport in the troposphere, and horizontal transport from subtropics and midlatitudes into the tropics and polar regions. The relative importance of these processes for an observed ^{7}Be surface concentration is difficult to determine [*Feely et al.,* 1988].

However, the concentration ratio ^{10}Be/^{7}Be is an ideal tool to indicate stratospheric air mass intrusions into the troposphere [*Raisbeck et al.,* 1981]. The source distributions of ^{7}Be and ^{10}Be are identical and both elements are transported and deposited in the same way, that is, the concentration ratio ^{10}Be/^{7}Be is independent of deposition. At the time of production the ratio ^{10}Be/^{7}Be is approximately 0.5 [*Lal and Peters,* 1967], but it increases rapidly, because the radioactive half life of ^{7}Be is much lower than that of ^{10}Be. Since the lifetime of a water-soluble tracer in the stratosphere is

Paper number 95JD01003.
0148-0227/95/95JD-01003$05.00

much larger than in the troposphere, stratospheric air masses are characterized by high values of $^{10}Be/^{7}Be$. Their transport through the tropopause into the troposphere causes a marked increase of the tropospheric $^{10}Be/^{7}Be$ concentration ratio.

The artificial ^{90}Sr serves as both a tracer for stratospheric circulation and the examination of air mass exchange between stratosphere and troposphere.

The transport model used in this study is driven by wind fields of the year 1990 assimilated by the European Centre for Medium Range Weather Forecasts (ECMWF). This allows for a direct comparison of model results with observations from 1990.

In the following section the transport model is presented. Afterward the three aforementioned radioactive tracer groups are described, and finally the simulation results are given.

Transport Model

The transport model numerically solves the continuity equation for the concentration of a tracer on a three-dimensional grid spanning the whole global atmosphere. The horizontal resolution of this grid is 7.83° in latitude (24 grid points) and 10° in longitude (36 grid points) [*Heimann,* 1995]. The present model version contains 19 layers using a hybrid coordinate system in the vertical dimension [*Rehfeld,* 1994].

The model is driven by observed 6-hourly horizontal wind data from 1990, analyzed by the ECMWF [*Rehfeld,* 1994]. The derivation of the air mass fluxes in zonal and meridional direction, which are needed by the model as input, from the ECMWF wind field analyses, together with an adjustment procedure ensuring the conservation of mass, is described by *Heimann and Keeling* [1989]. The vertical air mass flux is calculated in the transport model by mass continuity.

The model uses a numerical time step of 2 hours. In each time step, transport by advection is calculated by the numerical "slopes scheme," developed by *Russell and Lerner* [1981].

Two important subgrid scale vertical transport processes, cumulus convection and vertical turbulence, are parameterized in the transport model. Parameterization of vertical turbulence follows the scheme of *Louis* [1979], which is based on the calculation of the Richardson number. Cumulus convection is parameterized according to the scheme of *Tiedtke* [1989], which calculates the vertical convective mass flux in a cloud by the difference of entrainment and detrainment rates. The scheme is applied to three different types of convection (deep convection, typical for the tropics; shallow convection like the trade wind cumuli; convection in extratropical cyclones). The 6-hourly ECMWF analyses of geopotential, temperature, specific humidity, and horizontal wind components from 1990 are used as grid resolved variables.

The dry deposition flux of a tracer can be described as the product of a dry deposition velocity and the tracer concentration in the bottom model level. However, dry deposition is a very complicated process which depends on the meteorological condition of the atmosphere, the tracer properties and the type of the Earth's surface (ocean, land, vegetation). No generally accepted formulation of the dry deposition velocity exists [*Sehmel,* 1980]. Although some sophisticated dry deposition parameterization schemes have been developed [*Giorgi,* 1986; *Slinn,* 1976; *Slinn et al.,* 1978; *Chang et al.,* 1987], we follow a very simple approach in prescribing a constant dry deposition velocity of 0.1 $cm\,s^{-1}$ for all simulated radioactive tracers [*Feichter et al.,* 1991; *Brost et al.,* 1991]. Since the wet deposition is the primary removal process of the radioactive species regarded here [*Small,* 1959; *Todd et al.,* 1989; *Feichter et al.,* 1991; *Brost et al.,* 1991], this approach seems to be justified. However, in dry areas like the subtropics or polar regions, the percentage of dry deposition will increase, and the very simple parameterization employed here could no longer be appropriate.

Wet deposition of a tracer is a very complex process. The incorporation of aerosol particles by cloud droplets is a microphysical process, whereas the final removal of these aerosols by precipitation may reach synoptic scale dimensions. Basically, the wet removal rate of a tracer out of a grid box is described as the product of the tracer concentration in the grid box and a so-called "scavenging-efficiency" [*Junge and Gustafson,* 1957]. The wet deposition parameterization schemes for global transport models reported so far [e.g., *Levy and Moxim,* 1989; *Giorgi and Chameides,* 1986; *Joussoume,* 1990; *Kasibhatla et al.,* 1991] are based on this assumption. Merely different expressions for the scavenging-efficiency are used.

The scheme of *Kasibhatla et al.* [1991], which is applied in this study, sets the scavenging-efficiency λ as follows :

$$\lambda = R\rho_w / LH$$

where

- R precipitation rate out of a grid column, ms^{-1};
- ρ_w density of water, kgm^{-3};
- L cloud liquid water content, kgm^{-3};
- H vertical extension of precipitation, m.

The scheme distinguishes between stratiform and convective precipitation. For stratiform precipitation we set $L \equiv L_s = 1.5 \times 10^{-3}\ kg\,m^{-3}$, for the convective one $L \equiv L_c = 2.5 \times 10^{-3}\ kg\,m^{-3}$. These values are higher than those originally used by *Kasibhatla et al.* [1991] ($L_s = 0.5 \times 10^{-3}\ kg\,m^{-3}$, $L_c = 2 \times 10^{-3}\ kg\,m^{-3}$) as their values would result in too much scavenging in our model. Nevertheless, our values for L are still consistent with observations [*Warneck,* 1988; *Mason,* 1957]. The stratiform precipitation height is fixed at $H \equiv H_s = 3170\,m$ (seventh model level), the convective one at $H \equiv H_c = 8680\,m$ (eleventh model level). The precipitation fields used are daily 36-hour ECMWF predictions of stratiform and convective precipitation for the year 1990 with a horizontal resolution of 1.125 deg, integrated onto the transport model grid [*Arpe,* 1991].

The radioactive decay of a tracer is accounted for at every model time step through an adjustment of tracer concentration and the three spatial gradients within every grid box.

Radioactive Tracers in the Atmosphere

Natural Radioactivity Emitted From the Earth's Surface (Radon 222 and Lead 210)

The Earth's crust contains the radioactive element ^{238}U which decays over ^{226}Ra to the radon isotope ^{222}Rn. This element emanates out of the Earth's crust into the atmosphere. Radon 222 (mean radioactive lifetime of 5.52 days) is a water-insoluble inert gas which is lost from the atmosphere by radioactive decay to ^{210}Pb only [*Junge*, 1963]. Lead 210 atoms (mean radioactive lifetime of 32.3 years) become quickly attached to aerosol particles and are removed from the atmosphere primarily by dry and wet deposition.

The emission rate of ^{222}Rn depends on the concentration of its precursor in the decay chain (^{226}Ra) in the Earth crust, the meteorological conditions and the properties of the soil like water content, porosity, snow cover, and frost [*Mattsson*, 1970; *Dörr*, 1984; *Martell*, 1985; *Dörr et al.*, 1993]. The estimations of the global mean ^{222}Rn - emission vary between 0.72 [*Lambert et al.*, 1982] and 1.2 atoms cm^{-2}s^{-1} [*Turekian et al.*, 1977]. The oceanic ^{222}Rn emissions are about 2 orders of magnitude smaller than the continental emissions as a result of a smaller ^{226}Ra content of the ocean. Only approximately 2% of the atmospheric ^{222}Rn mass is of oceanic origin [*Wilkening and Clements*, 1975; *Peng et al.*, 1979].

In global transport models of the atmosphere the oceanic ^{222}Rn emission is usually neglected, and a constant emission rate from ice-free land surfaces is assumed [*Feichter et al.*, 1991; *Heimann and Feichter*, 1990]. This simple approach is justified on the grounds that local differences in the emission rate are assumed to average out over the large surface area of a model grid box [*Feichter et al.*, 1991]. We use a ^{222}Rn emission rate of 1 atom cm^{-2}s^{-1} in our simulation.

This is in agreement with the standard ^{222}Rn emission flux from land areas used by *Jacob and Prather* [1990]. However, they introduced a deviation from this standard value when changes in surface pressure, which generate a net flow of air through the soil, and soil freezing occur. In the case of freezing the standard ^{222}Rn emission flux is reduced by a factor of 3, based on a time series of ^{222}Rn emission flux measurements. A possible influence of evapotranspiration from vegetation and soil moisture content on the ^{222}Rn emission rate is neglected by *Jacob and Prather* [1990].

A quantitative interpretation of ^{226}Ra soil content in terms of ^{222}Rn emission is difficult because only a fraction of the decaying ^{226}Ra atoms releases ^{222}Rn to the soil gas. This fraction depends on the location of ^{226}Ra in the soil, that is, the soil type, and varies over a wide range from 10 to 50% [*Jacob and Prather*, 1990].

Many station observations of monthly ^{210}Pb concentration are available and can be compared with model results. Figure 1 shows the locations of these observing sites. Solid circles mark stations with observations from 1990 [*Larsen and Sanderson*, 1991; *Commissariat a l'Energie Atomique*, 1990a, b, c; D. Wagenbach, private communication, 1993]; crosses denote

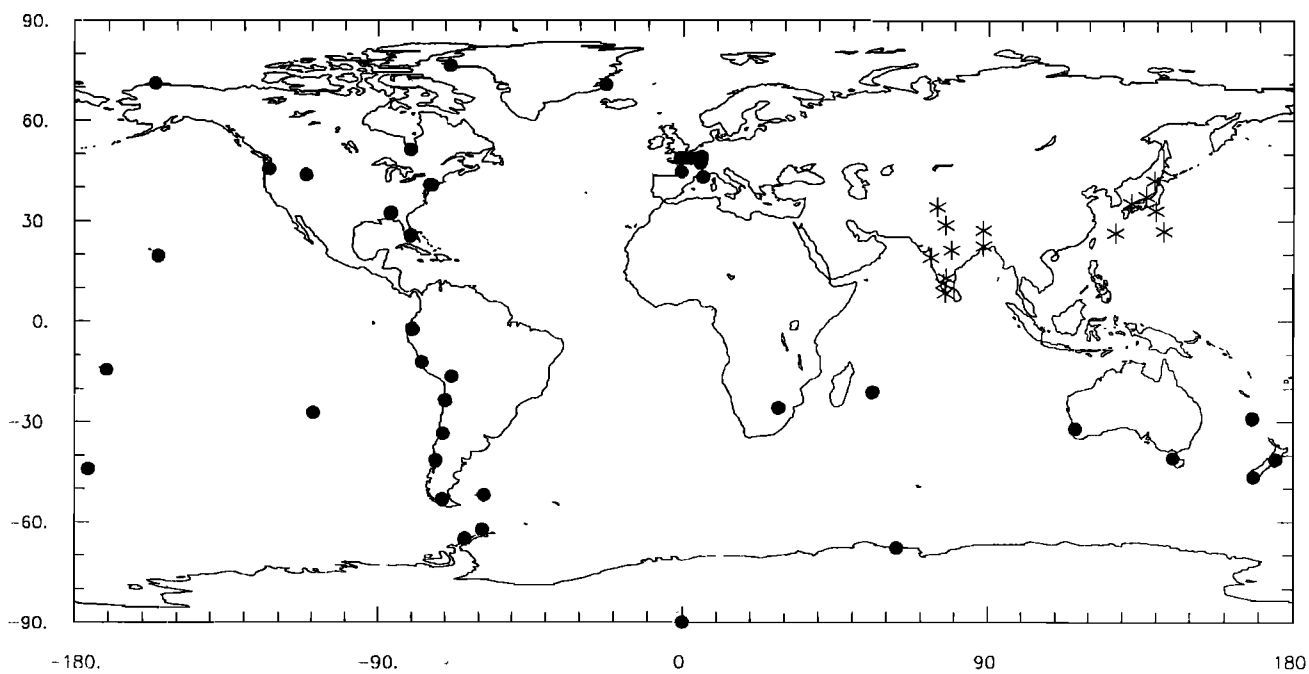

Figure 1. Monthly station observations of ^{210}Pb concentration. Solid circles mark stations with measurements from 1990; crosses denote sites with observations from other years (see text).

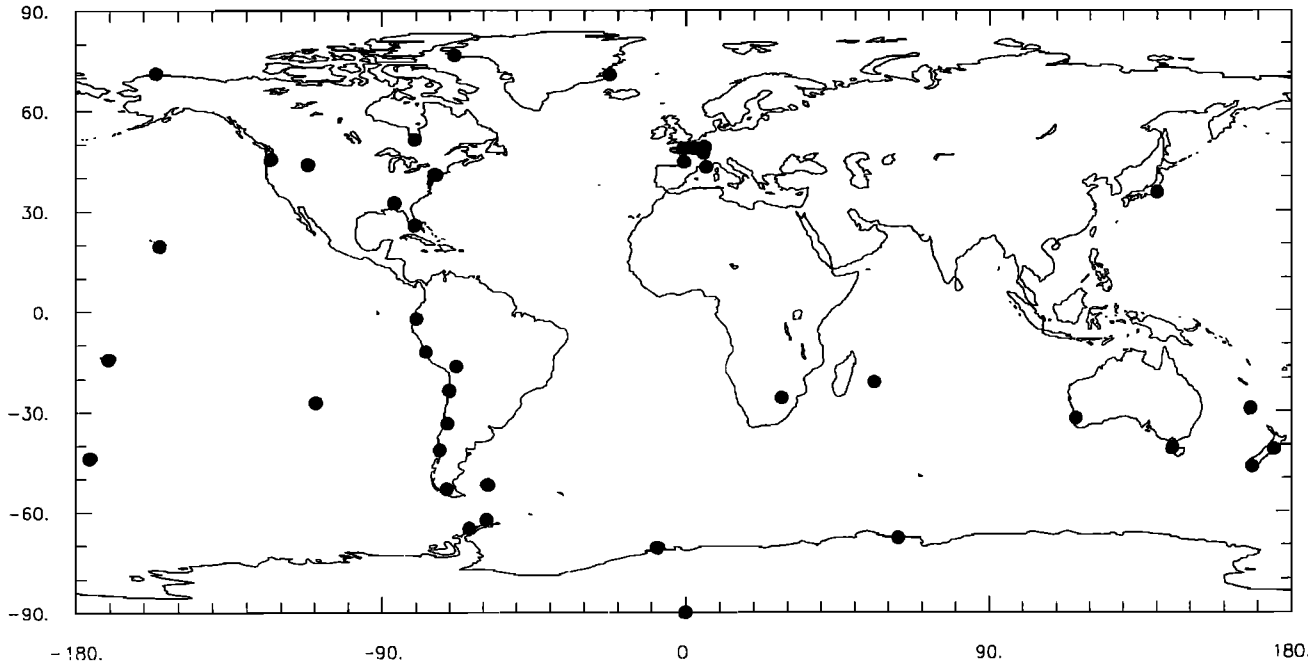

Figure 2. Locations of monthly ^{7}Be concentration observing sites (solid circles).

measurement sites with observations from other years [*Gopalakrishnan et al.*, 1973; *Tsunogai et al.*, 1988].

Natural Radioactivity Produced by Cosmic Radiation (Beryllium 7 and Beryllium 10)

The primary cosmic radiation, which is of galactic origin, consists primarily of protons and to a smaller degree of alpha particles and nuclei with atomic weights higher than 82 [*Friedlander*, 1989]. These cosmic particles penetrate into the atmosphere of the Earth. Because of the geomagnetic field this penetration is weak in the tropics but becomes more intense in polar regions [*Hillas*, 1972]. The zonal variation is weak [*Friedlander*, 1989].

The primary cosmic particles interact with atmospheric gas atoms during their penetration into the atmosphere [*Lal and Peters*, 1967]. Neutrons are formed by this process, and their interaction with atmospheric oxygen and nitrogen atoms produces ^{7}Be (mean radioactive lifetime: 76 days) and ^{10}Be (mean radioactive lifetime: 3.6×10^{6} years), about two thirds in the stratosphere and one third in the troposphere [*Lal and Peters*, 1967]. After their formation, ^{7}Be and ^{10}Be atoms are attached to aerosol particles (radii between 0.025 and 1 μm [*Brost et al.*, 1991]) and are removed from the atmosphere by dry and wet deposition [*McHargue and Damon*, 1991].

The inverse proportionality between the 11-year cycle of solar activity and the ^{7}Be (^{10}Be) production rate has been measured directly [*Lal and Peters*, 1967; *Hötzl et al.*, 1991; *Beer et al.*, 1990; *Lal*, 1987]. The decrease of ^{7}Be (^{10}Be) production from a sunspot minimum to a sunspot maximum varies between 70% in polar regions above 100 hPa and 7% in the lower equatorial atmosphere [*Lal and Peters*, 1967]. The calculation of the source distribution of ^{7}Be and ^{10}Be by *Lal and Peters* [1967], which is adopted here, is based on a period of high sunspot number (1948/1949), while the year 1990, observations used in this study, is also characterized by high solar activity [*Hötzl et al.*, 1991].

While many station observations of monthly ^{7}Be concentration from 1990 are available (Figure 2) [see *Larsen and Sanderson*, 1991; *Commissariat a l'Energie Atomique*, 1990a, b, c; *Abe et al.*, 1993; D. Wagenbach, private communication, 1993] ^{10}Be measurements are very sparse. The ^{10}Be concentration measured in the snow at the Georg-von-Neumayer station in the antarctic (70.58°S, 8.3°W), averaged over the period 1983 until 1986, is the only one available at the time of this study (D. Wagenbach, private communication, 1993). A thorough verification of model results against ^{10}Be observations is therefore impossible at present. Nevertheless, the model results of ^{10}Be/^{7}Be concentration distribution are a valuable tool to visualize the models air mass exchange between stratosphere and troposphere.

Artificial Radioactivity Due to Nuclear Weapon Tests (Strontium 90)

Systematic testing of nuclear weapons in the atmosphere began in the 1950s by the United States, the Soviet Union, and the United Kingdom [*Staley*, 1982]. The strongest tests occured in 1961/1962. After a longer period of no or insignificant testing (1963 - 1966), France and China resumed testing until the end of the 1970s [*Staley*, 1982], but the strength of these later tests was much smaller than that in the 1950s and early 1960s [*Enting and Pearman*, 1987]. One of the fallout products of these tests was ^{90}Sr (mean radioactive lifetime of 39.9 years).

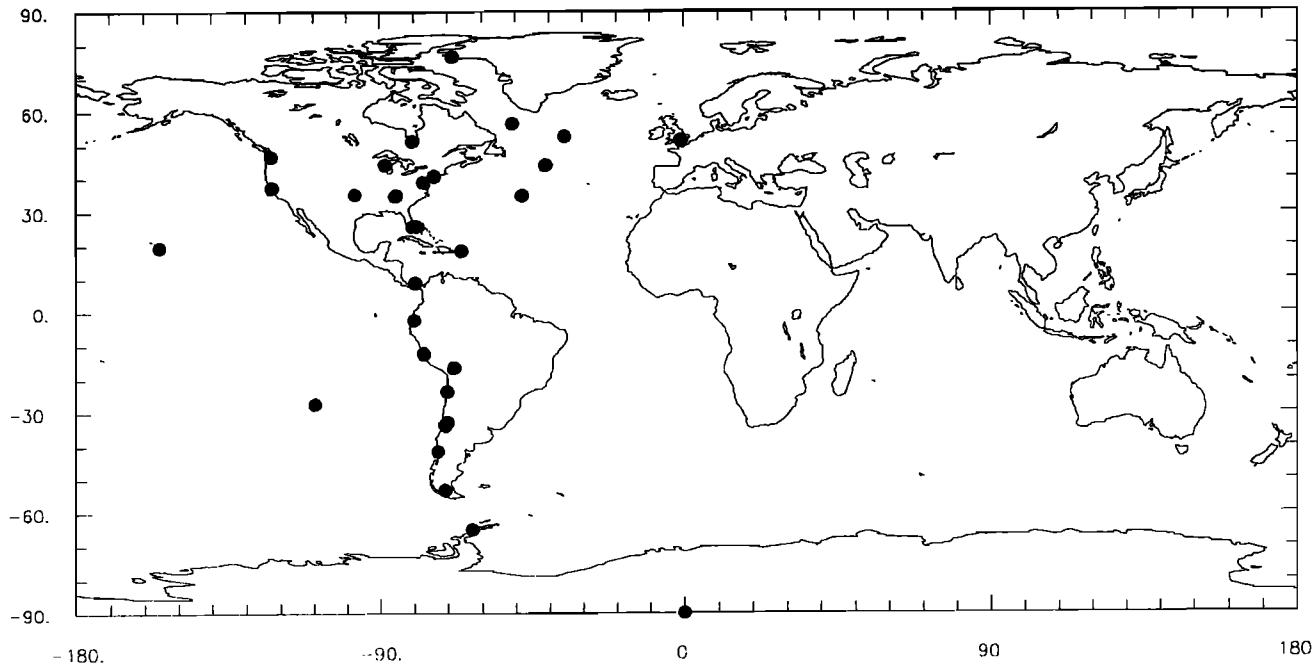

Figure 3. Locations of monthly ^{90}Sr concentration observing sites (solid circles).

Depending on the location and intensity of the test, a fraction of ^{90}Sr is deposited as local fallout, a further fraction is distributed within the troposphere, while some of the ^{90}Sr reaches the stratosphere [*Junge,* 1963]. *Machta and List* [1959] state that a test intensity of at least 1 MT TNT equivalent is needed to bring traceable amounts into the stratosphere.

After their formation, the ^{90}Sr atoms become attached to atmospheric aerosols (radii between 0.02 and 0.15 μm [*Feely et al.,* 1966]). The tropospheric ^{90}Sr is removed due to dry and wet deposition within a time interval of 1 - 2 months [*Machta and List,* 1959]. The stratospheric ^{90}Sr has a much longer atmospheric lifetime. It is transported through the tropopause into the troposphere and is finally removed by dry and wet deposition.

The fact that ^{90}Sr was brought into the atmosphere almost arbitrarily in time, space, and magnitude makes it difficult to use it as a tracer of atmospheric motions. Therefore we choose a period of no or insignificant testing for our tracer model simulation, that is, the period from 1963 to 1966. An initial stratospheric ^{90}Sr distribution must be derived from stratospheric ^{90}Sr measurements. Initial tropospheric ^{90}Sr concentrations can be neglected because of their removal within 1 - 2 months.

We constructed an initial ^{90}Sr distribution for January 1963 based on the measurements of the stratospheric ^{90}Sr concentration by the *U.S. Atomic Energy Comission* [1966]. All measurements from January 1963 are marked in a latitude-height coordinate system. A longitudinal dependence is ignored; that is, it is assumed that the zonal circulation of the stratosphere has eliminated any zonal inhomogenities introduced by the final tests at the end of 1962. Each hemisphere is divided into four latitude bands (0° - 15.65°, 15.65° - 39.13°, 39.13° - 62.61°, 62.61° - 90°). Within each zonal band all observations from the same height are averaged. A mean tropopause height, ranging from 8.8 km in the polar regions to 16.3 km in the tropics [*Holton,* 1979], is ascribed to each latitudinal band. Then the measurements were fitted within each band to a parabolic function with height. At tropopause height their value and the first derivative is set to 0 (boundary condition, neglection of tropospheric concentrations). The uppermost two model layers (index 18 and 19 at heights of 22 and 34 km, respectively) lie above the range of measurements and were set equal to the values of the 17 model level (19.5 km). Since no measurements are available for the latitudes south of 62.61°S, the results of the zone from 39.13°S to 62.61°S were extended to the south pole.

Figure 3 gives an overview about the measurement network of monthly surface ^{90}Sr concentration. All observing sites are located in the western hemisphere [*Feely et al.,* 1981; *Cambray et al.,* 1963, 1964, 1965, 1966, 1967].

Simulation Results

The model simulations presented in the following section are always based on the ECMWF wind and precipitation fields from the year 1990. If possible, the simulated tracer concentrations are compared with observations from 1990. The model results of ^{210}Pb are also compared with climatological ^{210}Pb data records. The ^{90}Sr simulation results are compared with observations from the investigated period 1963 - 1966.

Natural Radioactivity Emitted From the Earth's Surface (Radon 222 and Lead 210)

We have performed a 2-year model run, starting with an initial concentration of zero for ^{222}Rn and ^{210}Pb. The results presented here are based on the second model year when a stationary state is reached. One atom ^{222}Rn decays directly to one atom ^{210}Pb within the model time step of 2 hours since the isotopes in the reaction chain between ^{222}Rn and ^{210}Pb are very short lived [*Junge*, 1963].

Figure 4 shows the yearly mean of ^{210}Pb aerosol lifetime in the lowest (lower panel) and eleventh model layer (320 hPa, upper panel). In the lowest model level, lifetimes are everywhere less than 1 day since both dry and wet deposition work. In the eleventh model level a strong spatial variability of aerosol lifetime exists. The tropics and midlatitudes are characterized by low lifetimes due to high convective (tropics) and stratiform (midlatitudes) precipitation rates. Lifetimes in midlatitudes are generally less than 10 days and in the tropics even less than 5 days. On the other hand, the dry subtropics and polar regions show much higher aerosol lifetimes which can reach values of more than 100 days.

Figure 5 shows the percentage of dry ^{210}Pb deposition with respect to total ^{210}Pb deposition. This percentage remains low (under 10 percent) over the oceans, but is much higher over land areas. This is a result of the ^{210}Pb source distribution. In the very dry regions of the subtropics and antarctica the dry ^{210}Pb deposition becomes the dominant removal mechanism. However, dry deposition is parameterized very simply in our model. Therefore the calculated aerosol lifetimes in these dry regions may be regarded as questionable.

Figure 6 reveals the seasonality of aerosol lifetime. Figure 6 shows the zonal and vertical mean ^{210}Pb aerosol lifetime against latitude for January (solid line) and July (dashed line). The short lifetimes in the tropics

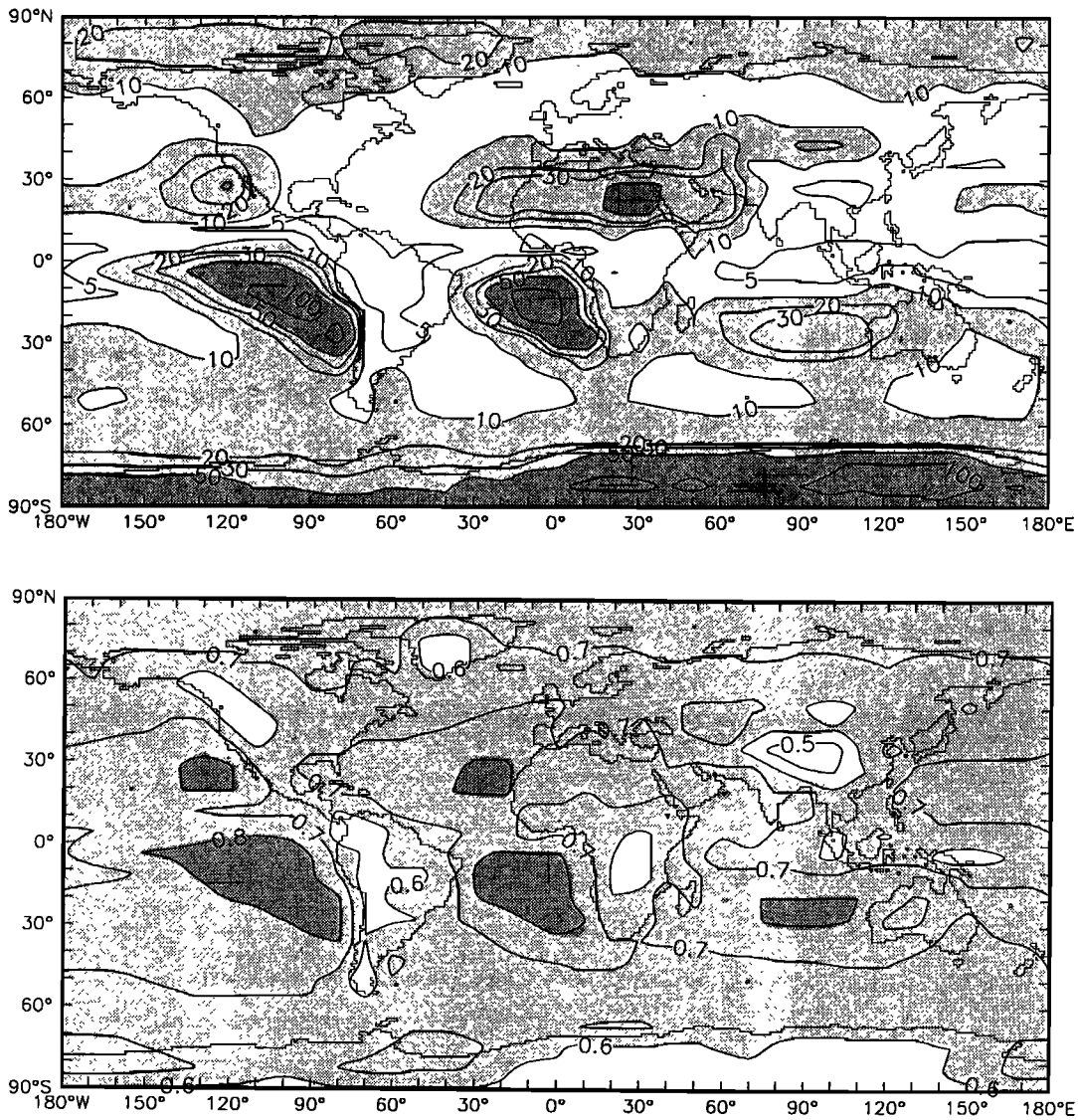

Figure 4. Yearly mean of ^{210}Pb aerosol lifetime (days) in the (upper) eleventh model level (320 hPa) and in the (lower) lowest model level.

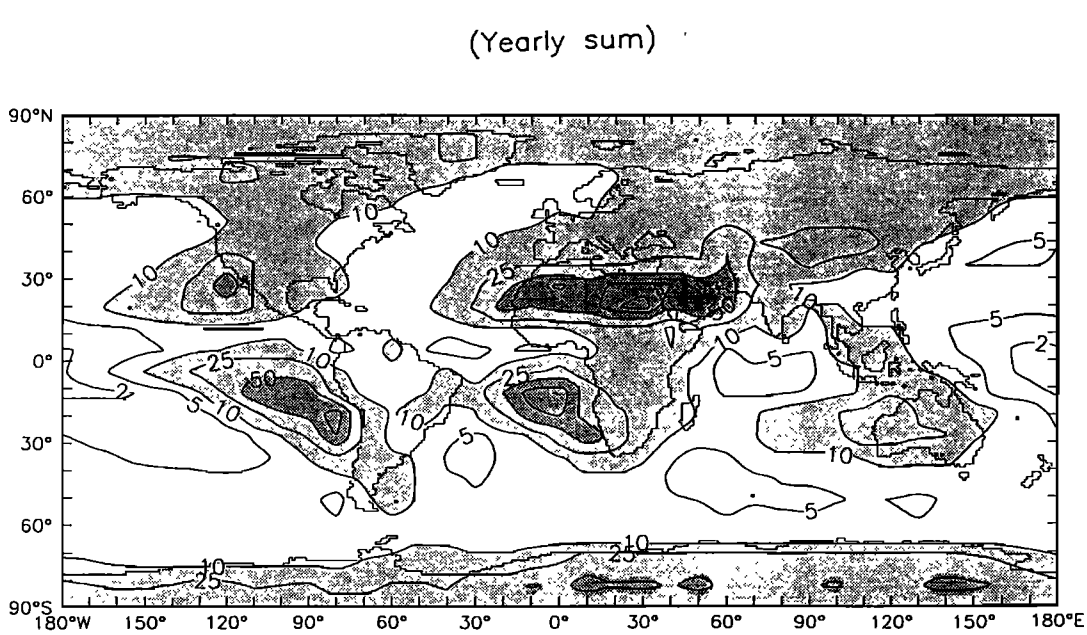

Figure 5. Percentage of dry ^{210}Pb deposition with respect to total ^{210}Pb deposition.

and midlatitudes and the long lifetimes in the subtropical and polar regions are evident. The seasonal shifting of the intertropical convergence zone (ITCZ) and midlatitude low-pressure trough causes the seasonality of the meridional pattern of the aerosol lifetime.

Figure 7 shows the ^{210}Pb concentration distribution in the lowest model layer for January (upper panel) and July (lower panel). The highest concentrations are found over land areas as a result of the ^{222}Rn source distribution, the lowest ones in the antarctica which is far away from any source region. Concentrations in the arctic are more than a factor of 2 higher in winter than in summer. This is due to an advective horizontal ^{210}Pb aerosol transport from midlatitudes which is also responsible for the arctic haze phenomenon [*Rahn*, 1981]. In spring the transport regimes change and ^{210}Pb aerosols are removed by precipitation preferably in midlatitudes [*Barrie et al.*, 1981].

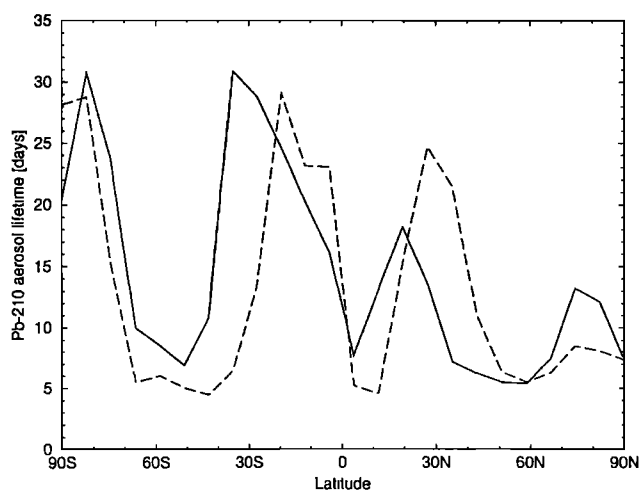

Figure 6. Zonal and vertical mean of ^{210}Pb aerosol lifetime (days) against latitude for January (solid line) and July (dashed line).

The monsoon circulation becomes evident by looking for the ^{210}Pb concentrations in southeast Asia and India. In winter the northeast monsoon carries dry and ^{210}Pb-rich air masses to this region whereas in summer the southwest monsoon removes ^{210}Pb aerosols efficiently due to its high precipitation amounts.

Figure 8 shows a comparison of modeled and observed ^{210}Pb concentration at six different locations (left column) together with a comparison of the ECMWF predicted precipitation rate, used by the transport model as input, and the observed precipitation rate (right column). No observed precipitation rates (WMO observing sites, data are supplied by the German weather service) from 1990 at the ^{210}Pb monitoring sites are available. If possible, measurements from a nearby site are used. Otherwise the precipitation climatologies of *Jaeger* [1976] and *Legates and Willmott* [1990] are taken.

Thule in Greenland represents an arctic station. The ^{210}Pb concentrations are high in winter and low in summer. As stated above (Figure 7), these high winterly concentrations are connected with an advective aerosol transport from midlatitudes (arctic haze). This transport regime changes in spring when the atmosphere becomes more convective. The transport model underestimates systematically this seasonality; that is, the modeled concentrations in summer are too high. This discrepancy is noticed also at other arctic stations (Point Barrow and Constable Point, not shown).

Four possible reasons can be suggested for these model deficiencies: Discrepancies between model used and observed precipitation, a wet deposition parameterization scheme which is too simple for the conditions in the cold arctic, neglecting of spatial and temporal variation

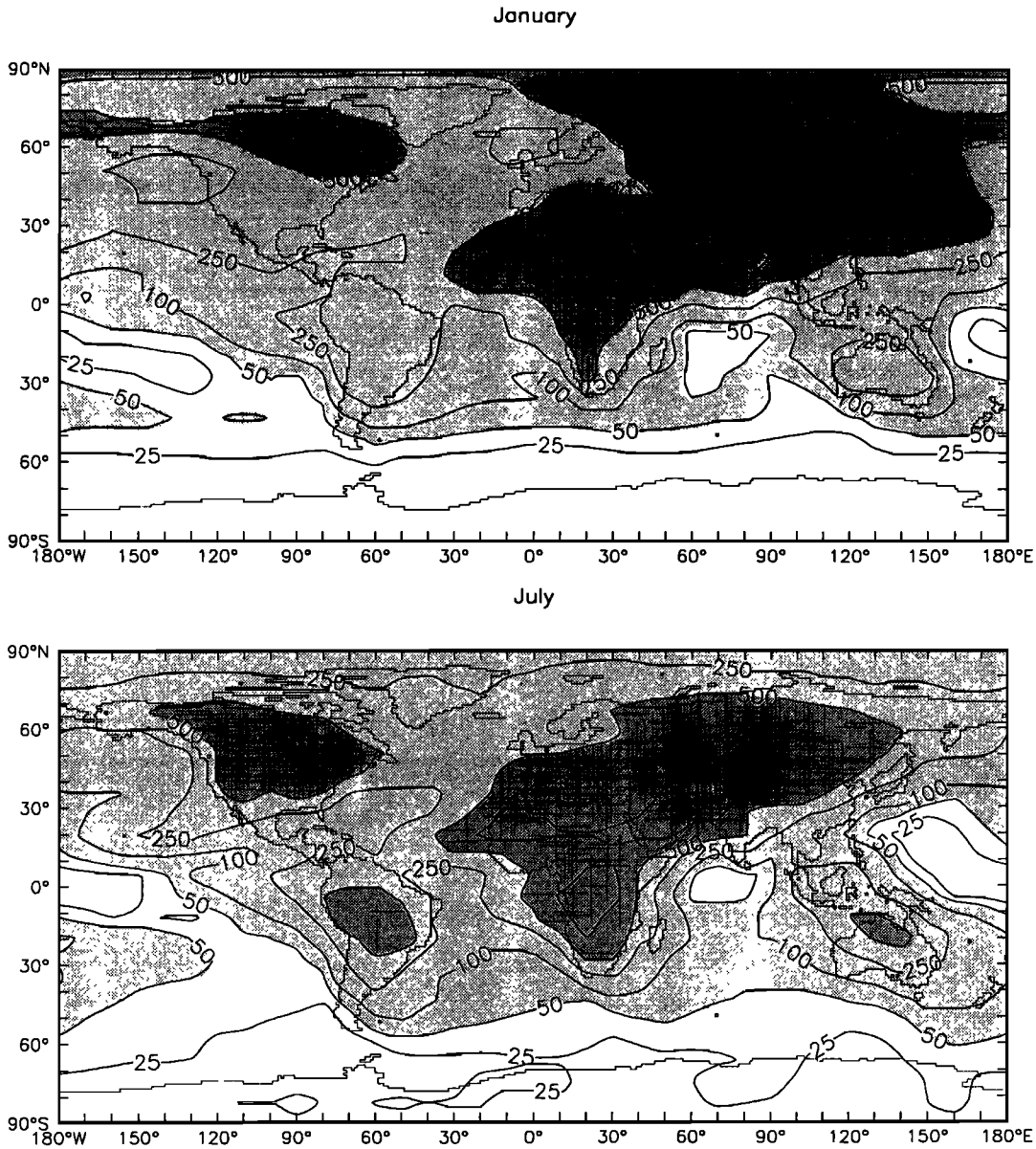

Figure 7. Lead 210 concentration distribution (μBq m^{-3}) in the lowest model level in (upper) January and (lower) July.

in ^{222}Rn emission and deficiencies in modeled aerosol transport from midlatitudes toward the arctic.

The model used ECMWF precipitation at the nearby site Egedesminde is often higher than the observed precipitation, but it results not in lower modeled ^{210}Pb concentrations. However, since precipitation shows a high spatial variability the results at Egedesminde may not be representative for Thule. Besides the rather simple formulation of wet deposition as employed here which might not be suitable for cold arctic precipitation regimes (snow, hail, sleet), also dry deposition becomes more important at low precipitation rates (Figure 5). Their simple parameterization could contribute to the discrepancies between observed and modeled ^{210}Pb values. A consideration of seasonality in the ^{222}Rn emission due to varying snow cover [*Dörr*, 1984] might also improve the simulation.

Okushiri (Japan) and Nagpur (India) are two observing sites which are strongly influenced by the monsoon circulation (right column of Figure 8). High precipitation amounts are found during the southwest monsoon in summer (June - September) whereas the northeast monsoon in winter (December - March) is very dry. At Nagpur the two precipitation climatologies and the ECMWF precipitation prediction compare very well, but at Okushiri the data set of *Legates and Willmott* [1990] shows an abnormal behavior (high winterly precipitation amounts). However, tha data set of *Jaeger* [1976] shows a good correspondence with the model used precipitation. In correspondence to this precipitation seasonality high ^{210}Pb concentrations are found in the dry winter season and low ^{210}Pb concentrations exist in the wet summer season. The agreement between observed and modeled concentrations is quite good.

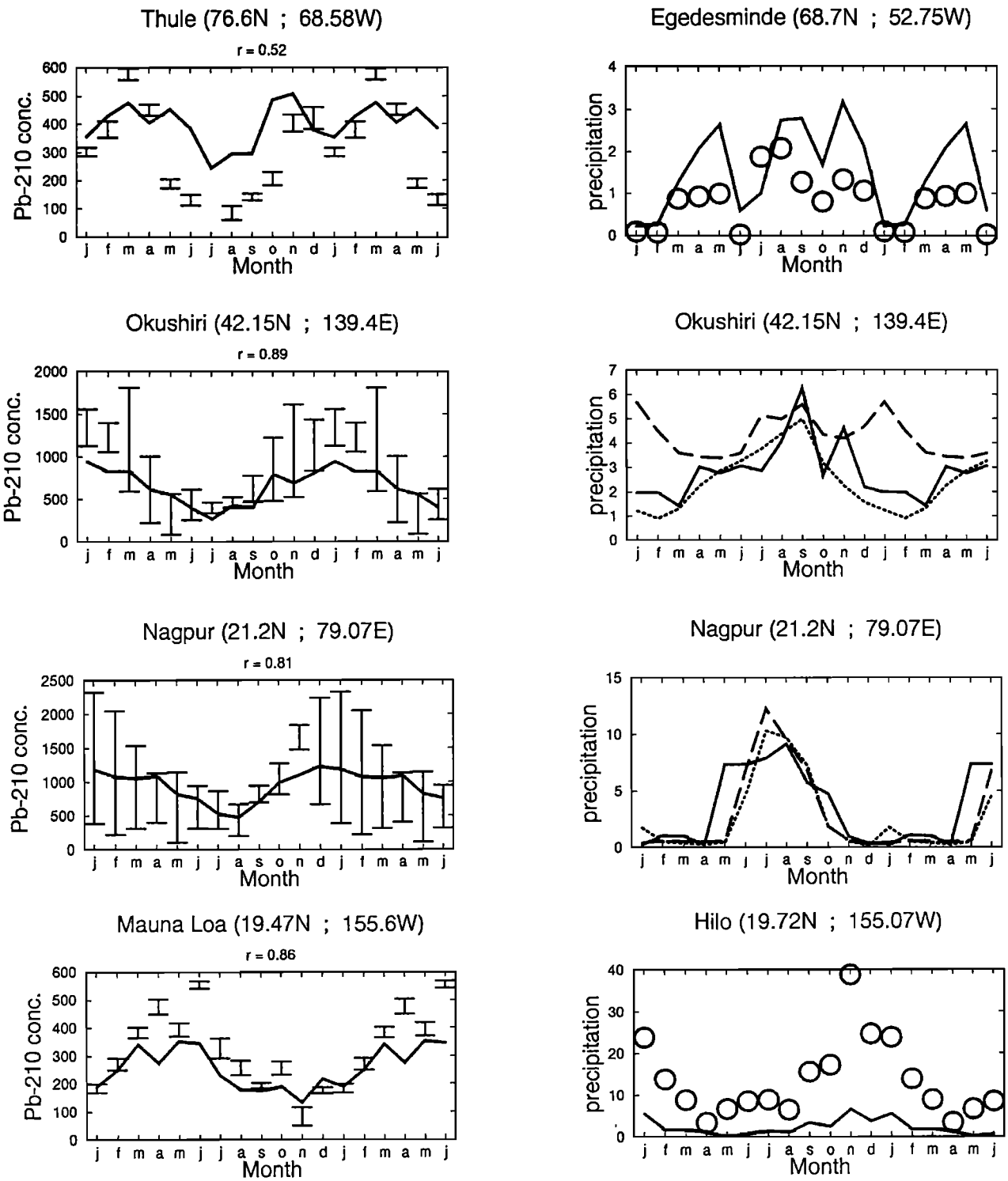

Figure 8. Comparison of observed and modeled monthly mean ^{210}Pb concentration (μBq m^{-3}) at six different locations (left column). The solid line represents the modeled values, the points denote observations. The error bars correspond to two standard deviations. The r value denotes the correlation coefficient. All measurements were carried out in 1990 with the exception of Okushiri (average over 1981 - 1983 [*Tsunogai et al.*, 1988]) and Nagpur (average over 1963 - 1966 [*Gopalakrishnan et al.*, 1973]). In the right column model used ECMWF precipitation forecasts (solid line) and observed precipitation rates (mm d^{-1}) are compared. No observations from 1990 at the stations are available. If possible, measurements from 1990 (WMO observing sites, data are supplied by the German weather service) at a nearby site are used (circles). Otherwise, the precipitation climatologies of *Jaeger* [1976] (dotted line) and *Legates and Willmott* [1990] (dashed line) are plotted. The first 6 months are repeated after the end of the year in order to reveal the seasonal cycle more clearly.

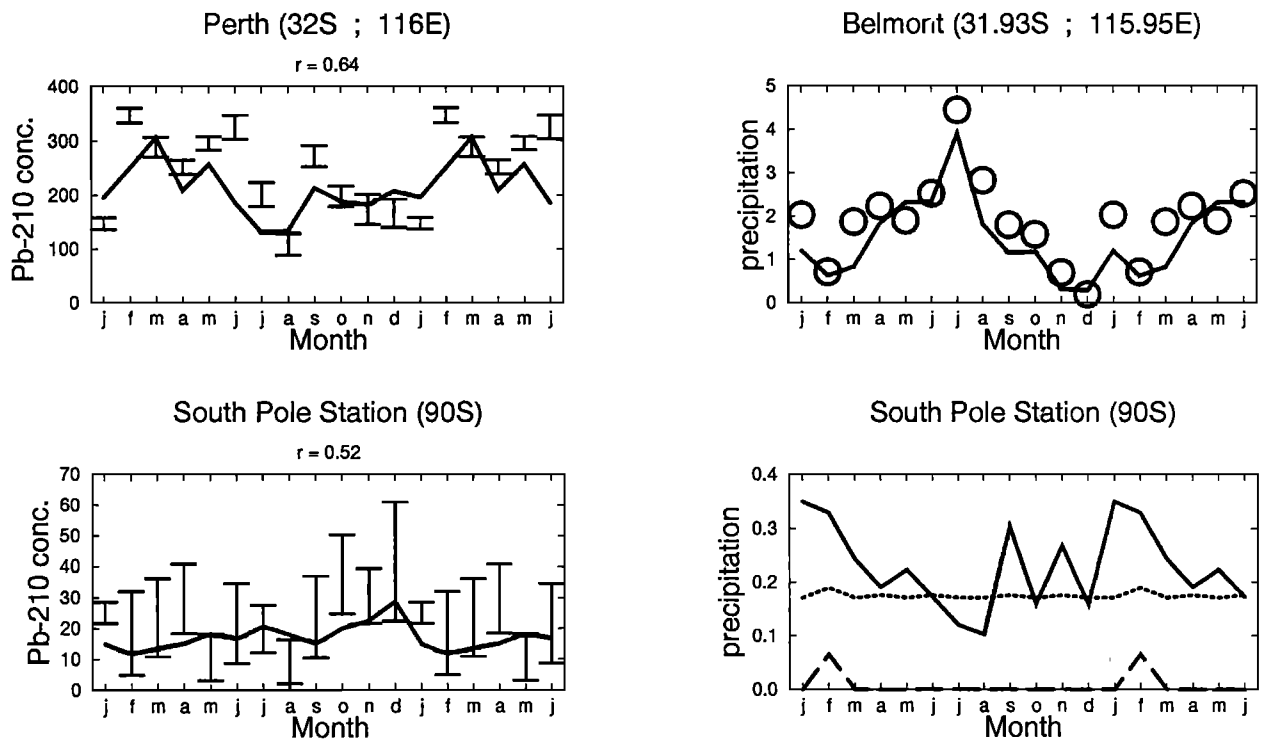

Figure 8. (continued)

At Mauna Loa a ^{210}Pb seasonality exists with high concentrations in spring and summer and lower ones in winter which is reverse to the seasonality found at higher latitudes. Because of its high elevation of 3400 m above sea level this station reflects the conditions in the middle troposphere rather than those in the planetary boundary layer (PBL). In summer the higher convective activity of the atmosphere decreases the ^{210}Pb concentrations in the PBL but increases them in the middle troposphere. Conversely, in winter the elevated Mauna Loa station is screened from the ^{210}Pb-rich lower tropospheric air masses. The model used ECMWF precipitation rate at the nearby station Hilo is considerably lower than the observed one. However, modeled and observed ^{210}Pb concentrations at Mauna Loa are in good agreement. Probably the high observed precipitation amounts at Hilo are caused by a local effect, like the orography, and are not representative for the Mauna Loa station.

At Perth, high ^{210}Pb concentrations exist in southern hemisphere summer (December - February) and low values in winter (June - August). This station is primarily influenced by the seasonality in precipitation (low summer and high winter values). The agreement between model used ECMWF precipitation and the observations is quite good.

The antarctic South Pole station shows a ^{210}Pb maximum in summer (December) and a minimum in winter (August). The seasonal cycle at this station is mainly influenced by transport processes from midlatitudes since the local ^{222}Rn (^{210}Pb) input is small (ice or water covered surfaces). In summer increasing amounts of ^{210}Pb aerosols are carried to the upper troposphere and are transported from midlatitudes toward the antarctic [*Lambert et al.*, 1990]. The precipitation rate at this station seems to be very uncertain. The two climatologies are much different. *Legates and Willmott* [1990] exhibit practically no precipitation, whereas *Jaeger* [1976] indicates a constant level of approximately 0.2 mm d^{-1} throughout the year. The model used ECMWF precipitation shows much more variability from month to month. However, the absolute precipitation amounts are very small and may have only a secondary effect on the local ^{210}Pb concentrations.

Natural Radioactivity Produced by Cosmic Radiation (Beryllium 7 and Beryllium 10)

We have started the transport model with an initial concentration of zero for ^{7}Be and ^{10}Be and let it run for 8 years (because of the long stratospheric lifetime of ^{10}Be) after which a stationary state is reached on annual average. The resulting concentration distributions of ^{7}Be and ^{10}Be were stored and used as initial fields for a final 1 year model run.

Figure 9 shows the ^{7}Be concentration distribution in the lowest model layer for January (upper panel) and July (lower panel). High concentrations are always found in the subtropics, especially over the Sahara. A combination of low precipitation and sinking air motion is responsible for that. Likewise high concentrations exist over the Himalaya as a result of its high elevation. Minima are found in the midlatitudes of the southern hemisphere (high stratiform precipitation amounts) and around the intertropical convergence zone (high convective precipitation rates). A pronounced seasonality exists over southeast Asia. High concentrations in winter

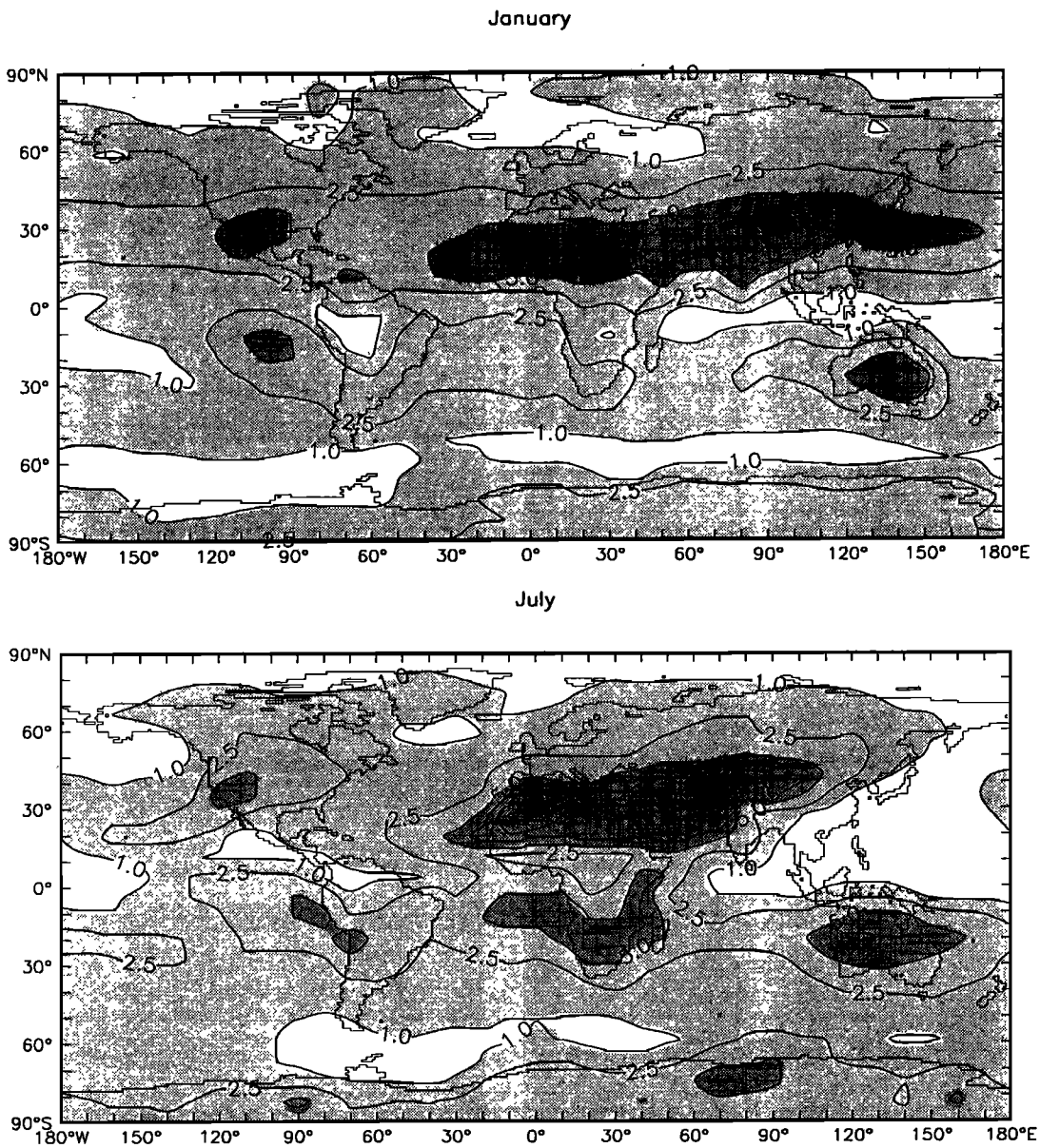

Figure 9. Beryllium 7 concentration distribution ($mBq\,m^{-3}$) in the lowest model level for (upper) January and (lower) July.

are connected with the dry northeast monsoon, whereas the low concentrations in summer are caused by the high rainfall rates of the southwest monsoon.

The usefulness of the concentration ratio $^{10}Be/^{7}Be$ in showing stratospheric mass intrusions into the troposphere becomes evident in Figure 10. It shows a meridional cross section of modeled zonal mean concentration ratio $^{10}Be/^{7}Be$ for March (upper panel) and October (lower panel). The stratospheric values of $^{10}Be/^{7}Be$ are much greater than the tropospheric ones due to the longer stratospheric tracer lifetime. Minima exist in the upper tropical troposphere. A strong vertical gradient characterizes the transition from troposphere to stratosphere, indicating the air mass exchange barrier at the tropopause. The low $^{10}Be/^{7}Be$ values are caused by the upward tropospheric air mass transport in the domain of the ITCZ.

A much different feature is found in midlatitudes. The strong vertical gradient at the tropopause vanishes and the values of $^{10}Be/^{7}Be$ are much higher than in the tropics. This indicates a more intense mass exchange between stratosphere and troposphere due to tropopause folding events. A pronounced seasonality of this mass transfer through the tropopause exists, especially in the northern hemisphere. In spring (March in northern hemisphere and October in southern hemisphere, respectively) the values of $^{10}Be/^{7}Be$ are much higher than in autumn (October in northern hemisphere and March in southern hemisphere, respectively). This seasonality is due to a vertical shifting of the tropopause height [*Staley*, 1982] and also to changes in the circulation [*Reiter*, 1975].

In spring the tropopause rises, so that decay products like ^{7}Be and ^{10}Be are transfered to the upper tro-

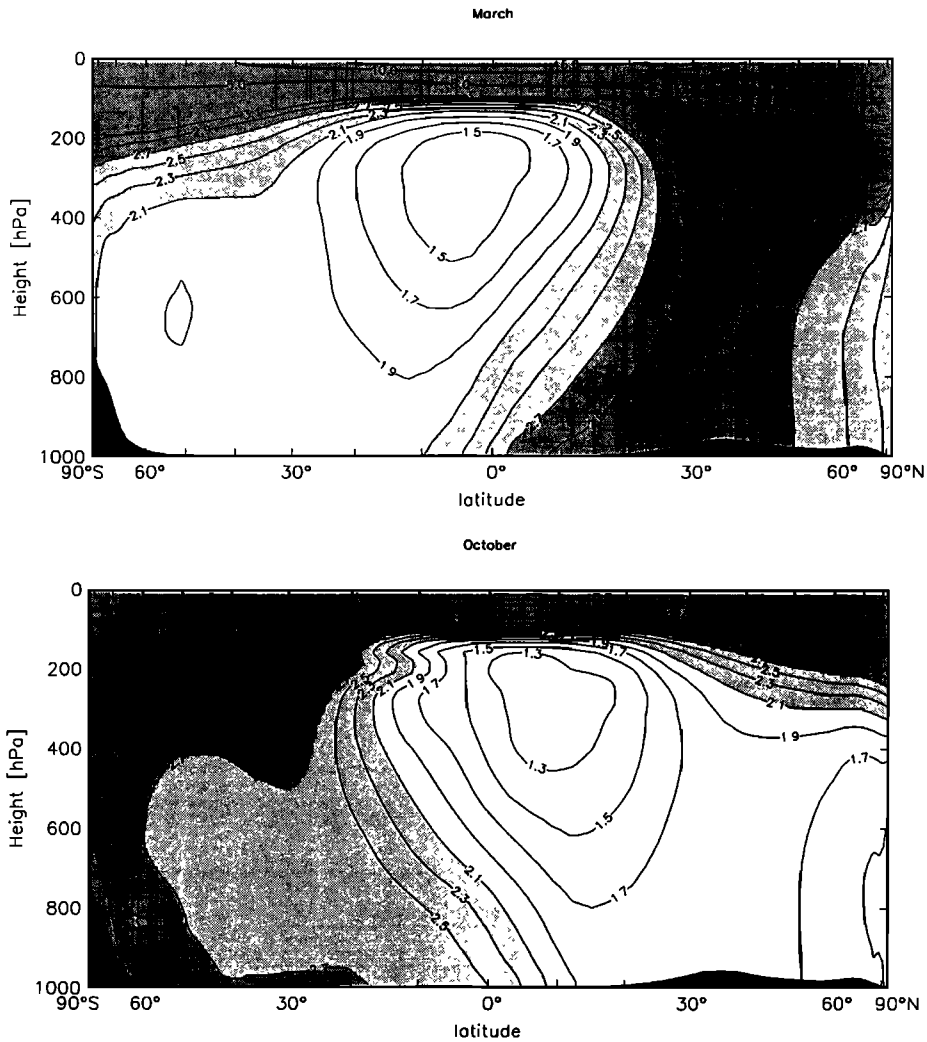

Figure 10. Meridional cross section of modeled zonal mean concentration ratio $^{10}Be/^{7}Be$ for (upper) March and (lower) October.

posphere and rapidly mixed downward. In autumn the reverse process occurs [*Staley*, 1982]. The transport of tropospheric air through the tropopause into the stratosphere by the tropical branch of the Hadley cell is highest in the winter season and lowest in summer. For reasons of continuity, the same amounts of stratospheric air will return into the troposphere in middle and high latitudes, thus contributing to the spring maximum in $^{10}Be/^{7}Be$ [*Reiter*, 1975]. Furthermore a seasonality in mass exchange between the stratosphere and the troposphere is introduced by the seasonal shifting of the subtropical and polar jet streams [*Reiter*, 1975].

Figure 11 shows the concentration ratio $^{10}Be/^{7}Be$ in the lowest model level for March (upper panel) and October (lower panel). Obviously, the seasonality of air mass exchange between stratosphere and troposphere is not confined to specific longitudes since the zonally distribution of the concentration ratio $^{10}Be/^{7}Be$ is rather homogeneous.

Figure 12 further elucidates the seasonality of air mass exchange between stratosphere and troposphere. It depicts the zonal mean concentration ratio $^{10}Be/^{7}Be$ as a function of latitude and season in the lowest (lower panel) and eleventh model layer (320 hPa, upper panel). Two marked spring maxima occur in the lowest model level, one in each hemisphere. However, the structure south of 60°S with two maxima (July and October) is not confirmed by the observations of $^{10}Be/^{7}Be$ (concentrations were measured in the snow) at the Georg-von-Neumayer station (70°S) in the antarctic (D. Wagenbach, private communication, 1993) as discussed later in this section.

In the eleventh model layer the northern hemisphere maximum occurs 1 month earlier (February) compared to the lowest model level. Stratospheric radioactive decay products which penetrate here into the troposphere require approximately one month to be mixed downward to the surface [*Raisbeck et al.*, 1981]. Afterward they are transported horizontally toward the tropics and subtropics as well as the polar regions.

Figure 13 shows a comparison of modeled and observed ^{7}Be concentration at six different locations (left column). In the middle column the predicted $^{10}Be/^{7}Be$ concentration ratio at the measuring site is shown. On

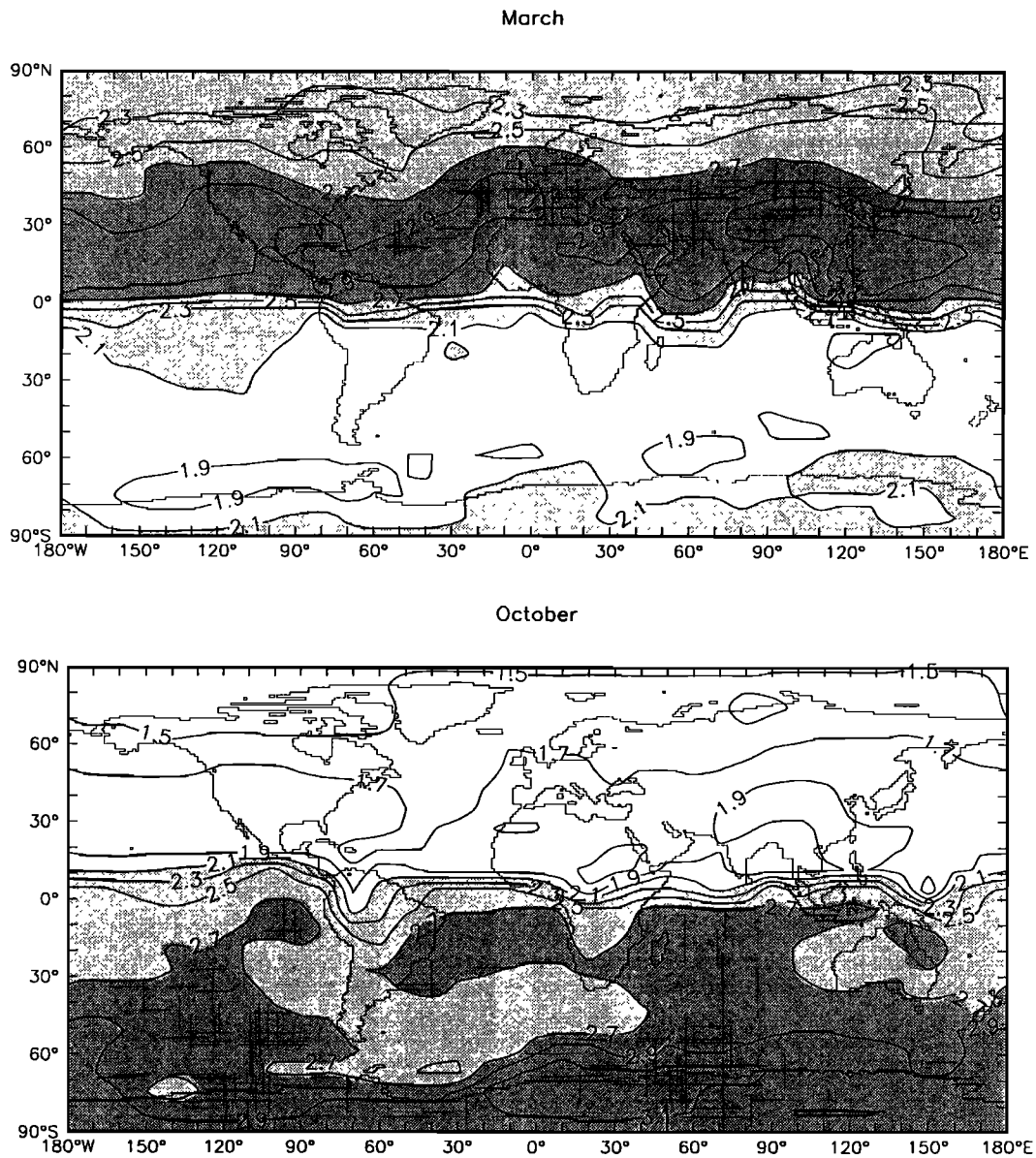

Figure 11. Concentration ratio $^{10}Be/^{7}Be$ in the lowest model level for (upper) March and (lower) October.

the right-hand side the model used ECMWF precipitation forecasts are compared with the observed precipitation rates (Figure 8).

At Barrow in Alaska a characteristic annual cycle with high winterly and low summerly ^{7}Be concentrations exists which is a little bit underestimated by the transport model. As stated already for ^{210}Pb, this cycle is due to an advective aerosol transport in winter from midlatitudes. The seasonality of modeled $^{10}Be/^{7}Be$ looks very similar to that of ^{7}Be concentration, that is, stratospheric ^{10}Be-rich air masses which penetrate into the troposphere in midlatitudes are transported toward the arctic. The model used ECMWF precipitation is often higher than the observations, but because of the generally low precipitation amounts the effect on the ^{7}Be concentrations should be small.

Rexburg is a continental station in the western central United States. A pronounced seasonality of ^{7}Be concentration is evident with a maximum in summer and a minimum in winter. Modeled values are systematically lower than the observed ones, perhaps due to the much higher model used precipitation rate (nearby station Helena). The maximum in summer is caused by the higher convective activity by which much more ^{7}Be aerosols are transported downward out of their source region [*Feely et al.*, 1988]. These ^{7}Be aerosols are not of stratospheric origin since the $^{10}Be/^{7}Be$ concentration ratio reaches a minimum in summer (middle column). The $^{10}Be/^{7}Be$ concentration ratio has a maximum in spring and it is reflected by a small secondary ^{7}Be concentration maximum in March (left side).

Miami is a subtropical station which is mainly in-

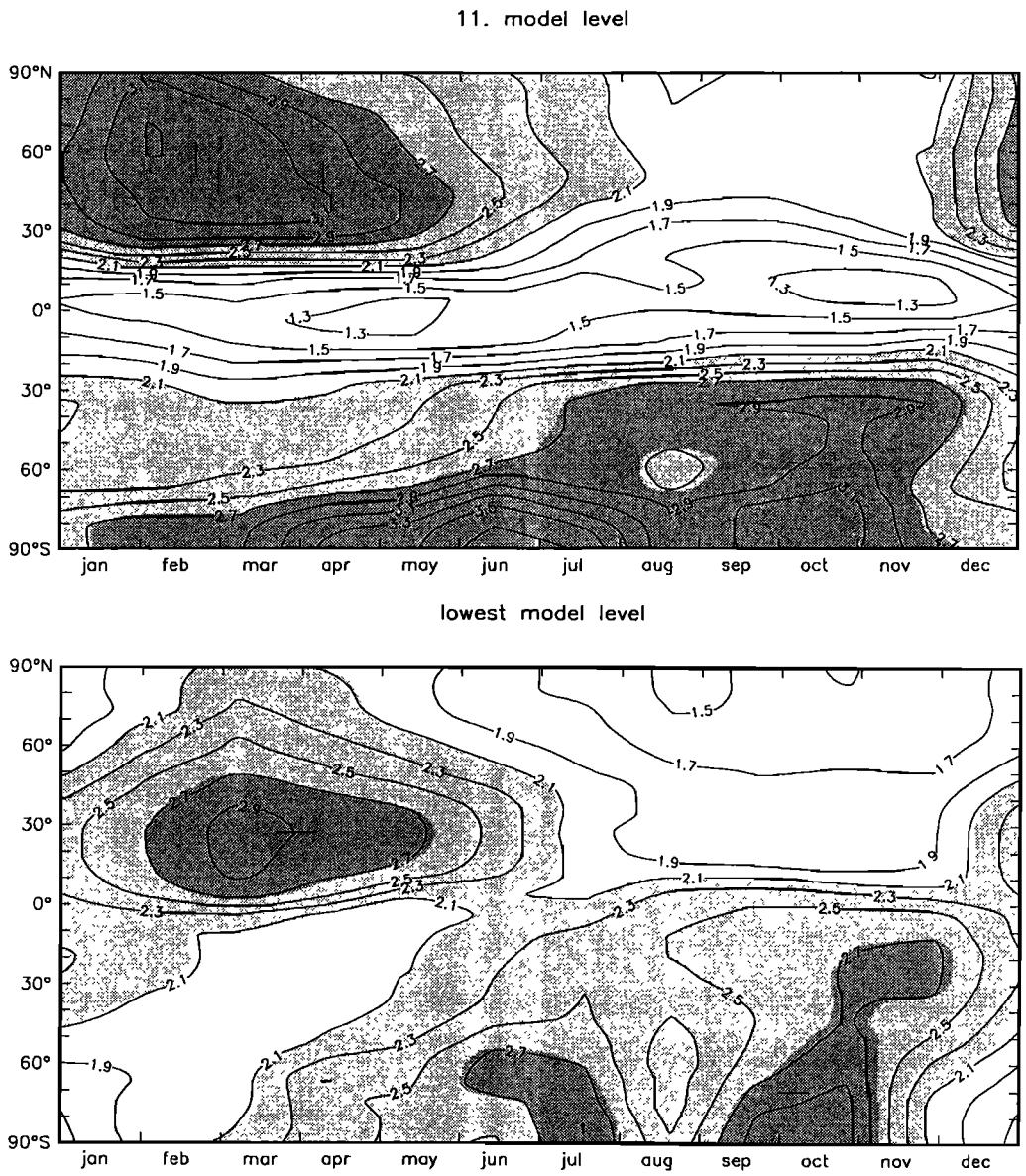

Figure 12. Zonal mean concentration ratio $^{10}Be/^{7}Be$ as a function of latitude and season in the (upper) eleventh model level (320 hPa) and (lower) lowest model level.

fluenced by the precipitation seasonality [*Feely et al.*, 1988]. The ^{7}Be concentrations are high in winter (low rainfall rates) and low in summer (high rainfall rates). The modeled seasonality of ^{7}Be concentration is much stronger than observed, although model used precipitation seasonality is obviously not (right panel). The modeled annual cycle of $^{10}Be/^{7}Be$ corresponds to that of ^{7}Be concentration. The ^{10}Be-rich stratospheric air masses enter the troposphere in midlatitudes and be advected toward the subtropics. It appears that the modeled seasonality of this transport is too strong thus causing the large amplitude in ^{7}Be concentration.

Lima in the southern hemisphere subtropics is obviously a station with a very dry climate [*Feely et al.*, 1988]. There was practically no precipitation measured in 1990, but the ECMWF precipitation predictions, used by the model, show a distinct seasonality with high summer (December - March) and low winter (June - September) values, maybe due to the seasonal shifting of the ITCZ. Because of this discrepancy a good agreement between modeled and observed ^{7}Be concentrations cannot be expected. The modeled ^{7}Be concentration seasonality seems to be primarily determined by the model used precipitation seasonality and to a lesser degree by the spring maximum (October) of $^{10}Be/^{7}Be$, that is, intrusion of stratospheric ^{7}Be into the troposphere. *Feely et al.* [1988] stated that the observed high ^{7}Be concentration in the southern hemisphere summer is due to stratospheric mass intrusions into the troposphere and intense vertical mixing in the troposphere. During the winter months wet mists, called garuas, cover the Pacific coast line. Air masses from

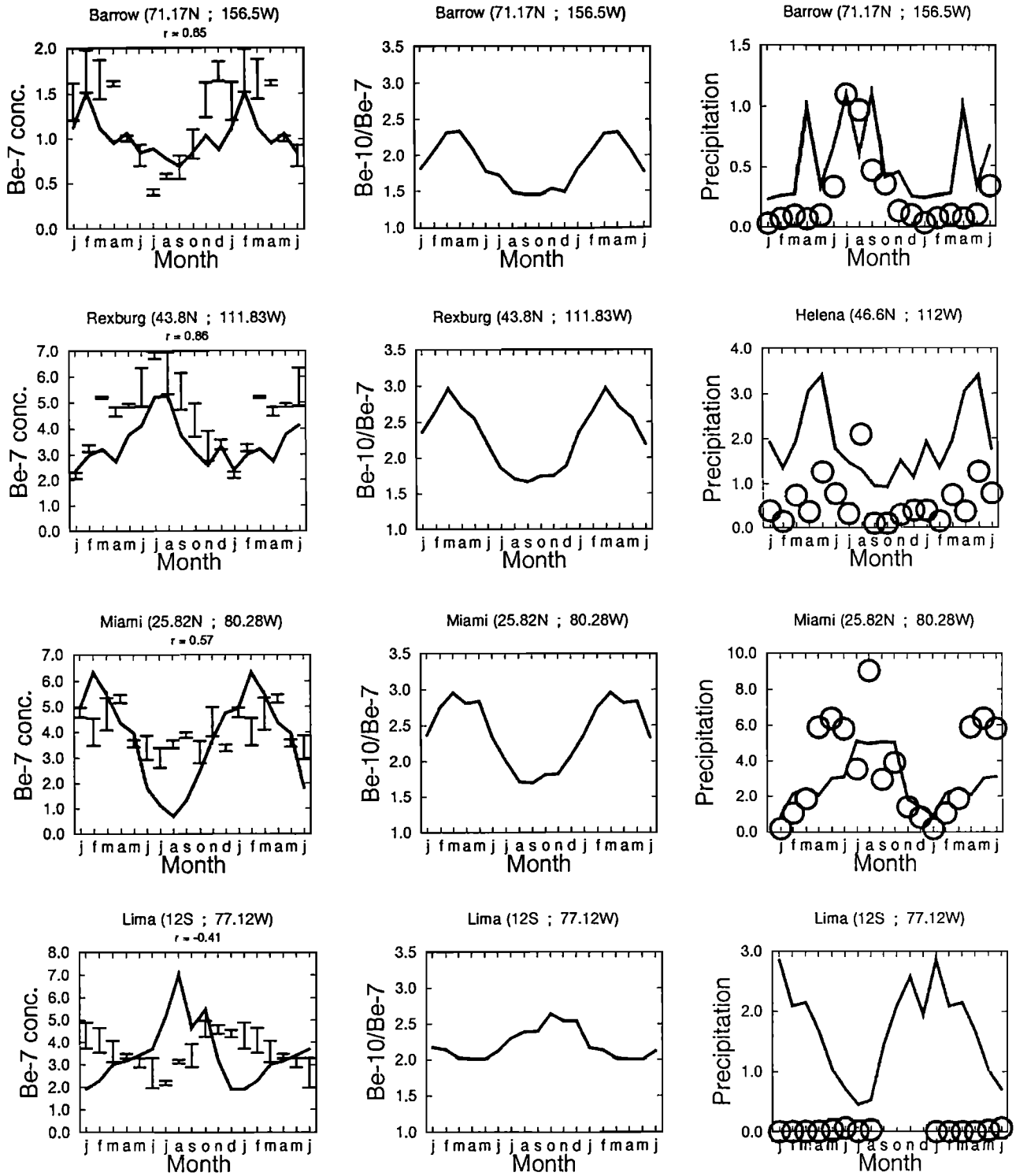

Figure 13. Comparison of observed and modeled monthly mean ^{7}Be concentration (mBq m^{-3}) at six different locations (left column). The solid line represents the modeled values; the points denote observations. The error bars correspond to two standard deviations. In the middle column the modeled concentration ratio of ^{10}Be/^{7}Be at the station is plotted (solid line). The observed ratio of ^{10}Be/^{7}Be (measured in the snow and averaged from 1983 to 1986) at the Georg-von-Neumayer station is shown by points with error bars representing two standard deviations. The r value denotes the correlation coefficient. In the right column model used ECMWF precipitation forecasts (solid line) and observed precipitation rates (mm d^{-1}) are compared. If possible, observations from 1990 (WMO observing sites, data are supplied by the German weather service), at or nearby the observing site, are used (circles). Otherwise, the precipitation climatologies of *Jaeger* [1976] (dotted line) and *Legates and Willmott* [1990] (dashed line) are plotted. The first 6 months are repeated after the end of the year in order to reveal the seasonal cycle more clearly.

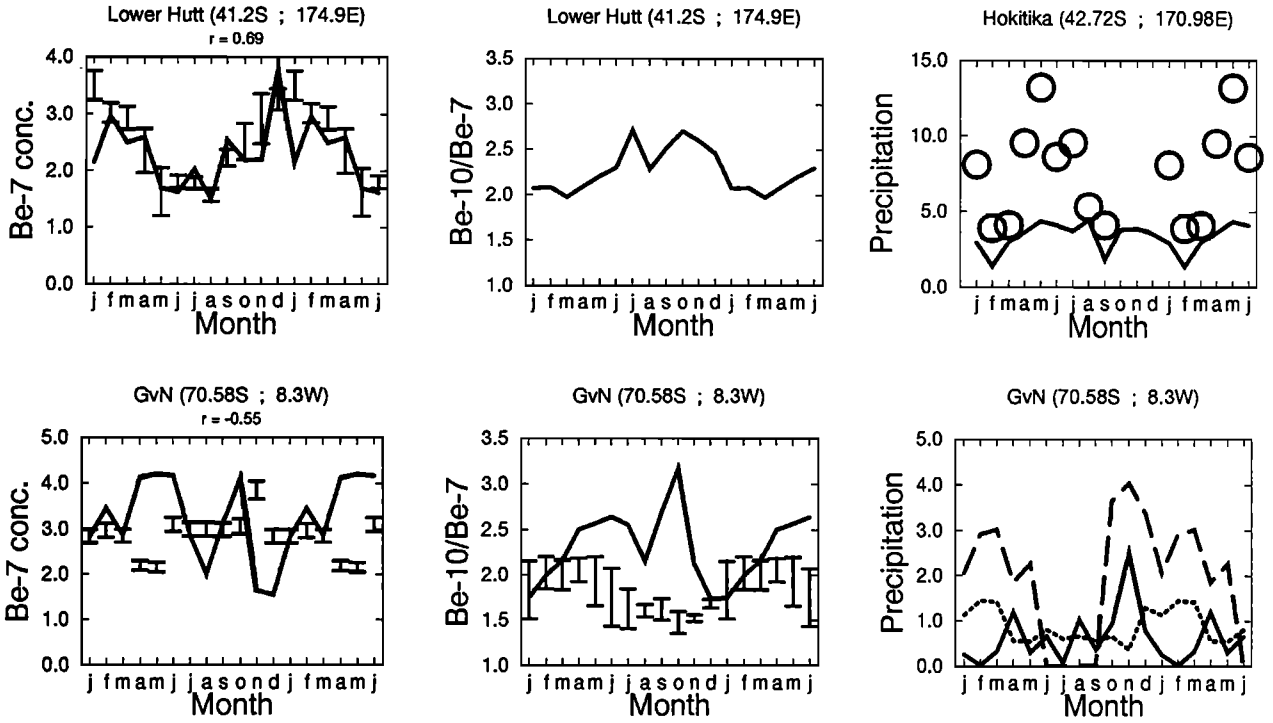

Figure 13. (continued)

the Pacific experience some washout before they reach the observing site downwind at Lima, therefore lowering the winter ^{7}Be concentration values [*Feely et al.*, 1988]. This subgrid scale phenomenon cannot be resolved by our coarse transport model.

Lower Hutt in New Zealand shows a quite good agreement between modeled and observed ^{7}Be concentration values, although the model used ECMWF precipitation is much lower than the observed precipitation. Low concentrations in southern hemisphere winter (June - September) correspond to high rainfall rates and vice versa. The fact that the discrepancy between model used and observed precipitation results in no discrepancy between modeled and observed ^{7}Be concentrations might be explained with different precipitation regimes in Lower Hutt and the nearby station Hokitika. The higher convective activity in summer (January - March) also increases the ^{7}Be concentration level at surface. The modeled ^{10}Be/^{7}Be ratio shows the aforementioned feature of two maxima (winter and spring, see Figure 12), as it is also obtained at the Georg-von-Neumayer station (see discussion below).

At the Georg-von-Neumayer station in the antarctic a large discrepancy between the observed ^{10}Be/^{7}Be (measured in the snow) and the modeled concentration ratio ^{10}Be/^{7}Be is obvious. The transport model shows two maxima, one in winter (June) and one in spring (October) (see Figure 12), whereas the observations show a maximum in southern hemisphere summer (February) and a minimum in spring (October). Since the concentration ratio ^{10}Be/^{7}Be is independent of removal processes this discrepancy may point to deficiencies in model transport regimes. Most probably the air mass exchange between stratosphere and troposphere is not accurately resolved in the antarctic ECMWF wind field analyses. However, it cannot be ruled out that also local meteorological effects like katabatic winds, which are not resolved by the transport model, are responsible for the discrepancy between the modeled and observed ^{10}Be/^{7}Be time series.

The modeled ^{7}Be concentration seasonality resembles the modeled ^{10}Be/^{7}Be seasonality. The observed ^{7}Be concentration shows a secondary maximum in summer (February), in correspondence to observed ^{10}Be/^{7}Be, but also a maximum in spring (November) which is in contrast to observed ^{10}Be/^{7}Be. However, the employed precipitation rates might be also inaccurate as indicated by the large discrepancies between the two climatologies and the ECMWF prediction for 1990.

Artificial Radioactivity Due to Nuclear Weapon Tests (Strontium 90)

We have started the transport model with the stratospheric ^{90}Sr concentration distribution of January 1963 and let it run for 4 years, that is, simulating the tracer development through the period from 1963 until 1966. Because of lack of adequate meteorological data, the transport model thereby was repeatedly cycled through the wind fields from the year 1990. This inconsistency might not be critical for our examination of the seasonality of air mass exchange between stratosphere and troposphere.

One point of interest is the time development of stratospheric ^{90}Sr mass which allows the determination of circulation regimes in the stratosphere. Figure 14 shows the development of northern stratospheric (up-

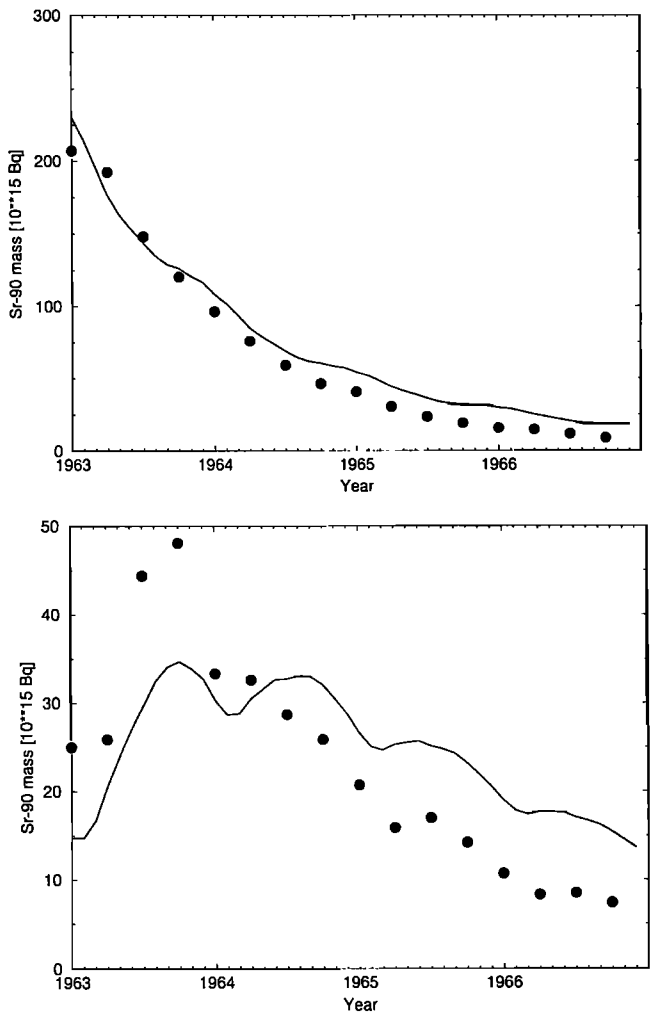

Figure 14. Time development of (upper) northern stratospheric and (lower) southern stratospheric ^{90}Sr mass (10^{15} Bq) during the 4-year simulation period from 1963 until 1966. The solid line represents the model; the points denote observations compiled by *Staley* [1982].

per panel) and southern stratospheric (lower panel) ^{90}Sr mass during the 4-year simulation period. The solid line represents the model; the points denote observations compiled by *Staley* [1982].

At the beginning of 1963 the northern stratospheric ^{90}Sr mass is about 1 order of magnitude larger than the southern stratospheric ^{90}Sr mass. It decreases continually as a result of mass transport through the tropopause and across the equator into the southern stratosphere. Southern stratospheric ^{90}Sr mass increases until October 1963 before it decreases just as in the northern stratosphere, that is, during the first 10 months of simulation the interhemispheric mass transport from the northern stratosphere is greater than the mass exchange through the tropopause into the southern troposphere. However, the ^{90}Sr mass decreases not continually since October 1963 but shows a seasonality with a temporary increase in southern hemisphere winter. This is due to the seasonality in air mass exchange between stratosphere and troposphere which is much more intense in spring and summer (see discussion below).

Although radioactive decay products are not distributed homogeneous in the stratosphere and troposphere, a simple four-box model (stratosphere and troposphere of northern and southern hemisphere) may be employed to summarize the global ^{90}Sr dispersal [*Staley,* 1982]. Expressions for the mean residence lifetime of mass transfer through the tropopause T_T and across the equator T_E, respectively, can be derived [*Staley,* 1982]. This mean residence lifetime gives the time interval during which an initial tracer mass input into a box is reduced to a fraction $1/e$ (Table 1).

The agreement between model and observations relative to interhemispheric mass exchange is quite good, whereas the modeled mass transport through the tropopause is slower than observed (Figure 14).

Figure 15 shows the zonally averaged ratio of the monthly mean ^{90}Sr concentration with respect to the yearly mean ^{90}Sr concentration as a function of latitude and season. The upper panel represents the conditions in the lowest model layer; the lower panel shows the surface observations. All measurements within 10 deg latitude bands were averaged, assuming that they are representative for that zonal band. The ratio is averaged over the time period 1964 - 1966.

A characteristic northern hemisphere spring maximum and autumn minimum of this ratio is obtained in the model as well as in the observations; that is, the air mass exchange between stratosphere and troposphere reaches its maximum during spring time and is minimal in autumn. The observations show a distinct time delay of this maximum with increasing latitude which is much weaker in the model. In the southern hemisphere a spring maximum (October) is also modeled and observed for latitudes north of 40°S. South of 40°S the model shows a structure of two maxima (winter and spring), which was also found for $^{10}Be/^{7}Be$ (Figure 12), whereas the observations between 40° and 50°S seem to indicate a summer maximum (February). However, no observations are available from southern polar latitudes; that is, there is no evidence that the observed ^{90}Sr seasonality is similar to the $^{10}Be/^{7}Be$ seasonality at the Georg-von-Neumayer station.

Conclusions

A global three-dimensional transport model of the atmosphere was used in this study to simulate the distribution of natural (^{210}Pb, ^{7}Be, ^{10}Be) and artificial

Table 1. Mean Residence Lifetimes for Stratospheric ^{90}Sr Mass Exchange Through the Tropopause T_T and Across the Equator T_E

	Staley [1982]	Transport Model
T_T	1.4	1.93
T_E	3.9	3.97

Lifetimes are in years.

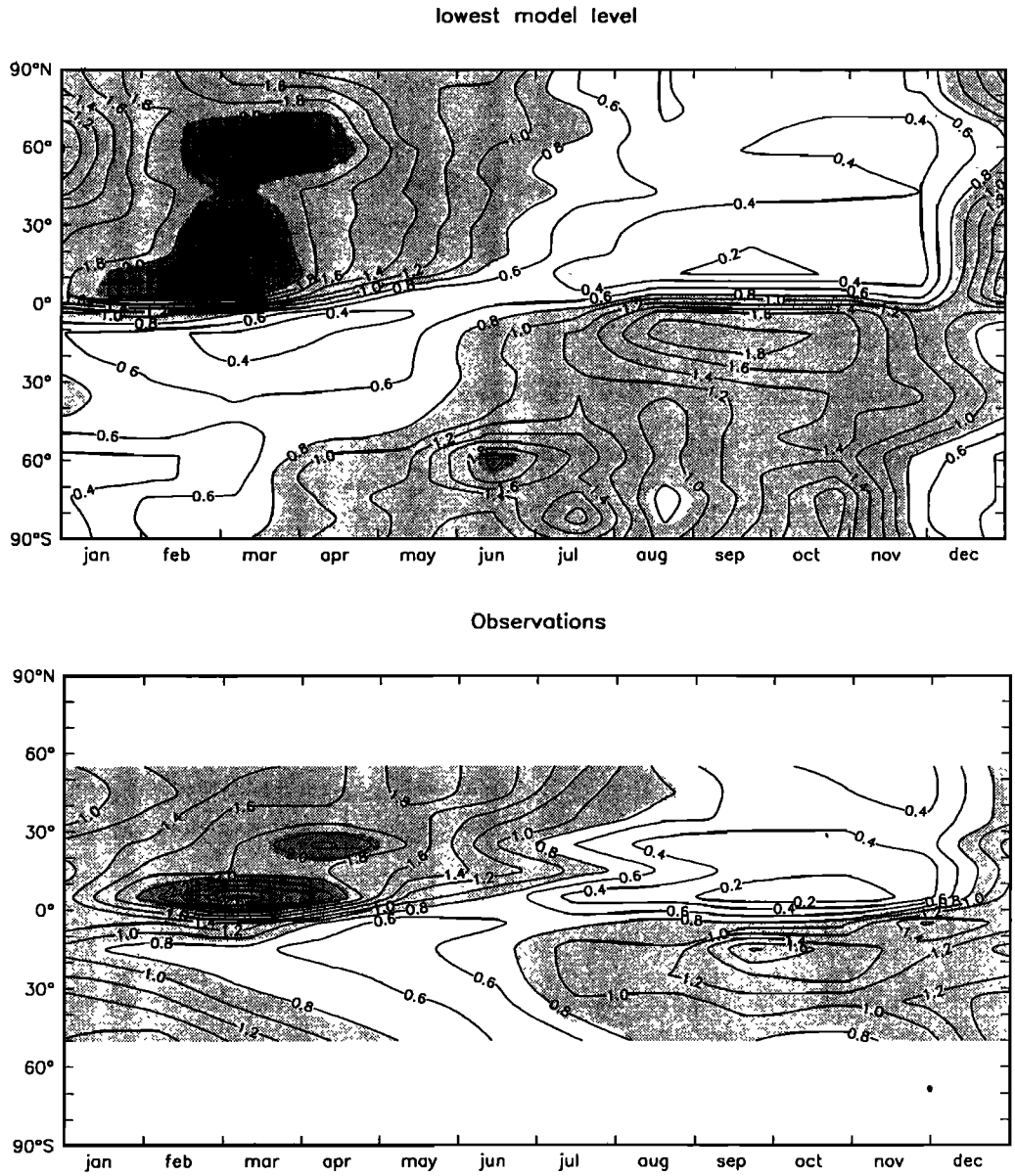

Figure 15. Zonal averaged ratio of the monthly mean ^{90}Sr concentration with respect to the yearly mean ^{90}Sr concentration as a function of latitude and season. The upper panel represents the conditions in the lowest model layer; the lower panel shows the surface observations. All measurements within 10 deg latitude bands were averaged, assuming that they are representative for that zonal band. The ratio is averaged over the time period 1964 - 1966.

(^{90}Sr), radioactive, water-soluble, aerosol-borne tracers in order to depict atmospheric transport processes and to test the models ability of reproducing these. The radioactive tracers have a well-known source-sink distribution and many observations are available to be compared with model results.

^{210}Pb, the decay product of the water-insoluble, short-lived inert gas ^{222}Rn emanating out of the Earth's crust, permits the investigation of transport processes in the lower troposphere. The cosmic ^{7}Be and ^{10}Be are useful for the examination of transport phenomena in the whole troposphere. The concentration ratio $^{10}Be/^{7}Be$ is an ideal tool to point out stratospheric air mass intrusions into the troposphere. The artificial ^{90}Sr serves as a tracer for stratospheric circulation regimes and is useful to investigate air mass exchange between stratosphere and troposphere. The attachment of these radioactive isotopes to aerosols allows the investigation of their lifetime in the atmosphere.

In general, the model reproduces the observed distributions reasonably well except for the polar regions. Modeled arctic ^{210}Pb and ^{7}Be concentrations are too high, while the seasonality is underestimated, especially for ^{210}Pb. In the antarctic a strong discrepancy between modeled and observed concentration ratio $^{10}Be/^{7}Be$ is found. The observations show a maximum of $^{10}Be/^{7}Be$

in summer whereas the model shows two maxima, one in winter and one in spring.

Several reasons may be suggested for these discrepancies in polar regions: (1) Deficiencies in the ECMWF wind fields by which the transport model is driven, (2) differences between true and model used precipitation, (3) inadequate dry and wet deposition parameterization schemes which are too simple to reproduce the conditions in the cold polar regions and (4) uncertainties in the tracer source distributions.

On the basis of our model simulations we conclude that the air mass exchange between stratosphere and troposphere may be not accurately resolved in the ECMWF wind field analyses south of 60°S and causes therefore the discrepancy between the observed and modeled concentration ratio of $^{10}Be/^{7}Be$.

We believe that the ECMWF precipitation forecasts represent the best data set available at present for carrying out such simulations of water-soluble tracers. However, the German weather service currently is preparing precipitation fields which take into account all observations of a particular year. These precipitation fields might help to improve the results in the arctic and antarctic.

Obviously, more sophisticated wet deposition parameterization schemes are needed. The scheme used in this study might be improved if informations about the vertical distribution of water vapour condensation were available. Furthermore, orographic effects on precipitation, as they occured for instance in the western part of the Andes (Lima), should be taken into account. These refined wet deposition parameterization schemes must be tested with the radioactive tracers to look for a possible improvement of simulations, especially in the polar regions. However, this paper has shown that reasonable tracer concentration and deposition distributions can be obtained even with a rather simple wet deposition parameterization scheme.

A refinement of the dry deposition parameterization (consideration of surface type, meteorological conditions, and tracer properties) with particular emphasis on polar regions and the subtropics is needed as the percentage of dry deposition with respect to total deposition increases in the arctic and antarctic due to low precipitation.

A consideration of seasonality in ^{222}Rn emission instead of prescribing a uniform emission rate might also improve the ^{210}Pb model results in the arctic. An annual cycle of ^{222}Rn emission probably exists due to a frozen surface in winter and a thawing one in summer.

Evidently, the validation of three-dimensional global model simulations requires extensive data sets. While the presently existing database of ^{7}Be and ^{210}Pb is sufficient to investigate the model performance in many key areas, there nevertheless exist large gaps mostly in polar and tropical regions. As demonstrated in this paper, especially, the $^{10}Be/^{7}Be$ ratio constitutes an interesting tracer to assess exchanges between the stratosphere and the troposphere. Compared to other stratospheric tracers (e.g., ozone) it has the advantage of not being subject to chemical reactions. Unfortunately, ^{10}Be measurements are still very sparse but would be very valuable in future model validation studies.

Acknowledgments. We thank J. Feichter for helpful discussions and for providing us with radioactive isotope measurement data. E. Roeckner, K. Arpe, U. Schulzweida, W. Welke, and I.Jessel assisted in preparing the ECMWF data. The ECMWF data were obtained from the German weather service in Offenbach. R.J. Larsen and R. Leifer from the Environmental Measurements Laboratory in New York as well as C. Johnson from the United Kingdom Atomic Energy Authority kindly provided us with ^{7}Be and ^{90}Sr observational data. Furthermore, we thank D. Wagenbach from the University of Heidelberg for the radioactive measurements at the Georg-von-Neumayer station in the antarctic. The transport model development was funded partly with support from the European Comission under contract EV5V-0120.

References

Abe, M., K. Kurotaki, S. Shibata, H. Takeshita, and S. Abe, Trends analysis of past ten years: Changes of radioactive substances in the atmosphere at Chiba, Japan, paper presented at International Symposium on Applications of Isotope Techniques in Studying Past and Current Environmental Changes in the Hydrosphere and the Atmosphere, Int. Atomic Energy Agency, Vienna, April 1993.

Arpe, K., The hydrological cycle in the ECMWF short range forecasts, *Dyn. Atmos. Oceans, 16,* 33 - 59, 1991.

Barrie, L.A., R.M. Hoff, and S.M. Daggupaty, The influence of mid-latitudinal pollution sources on haze in the Canadian arctic, *Atmos. Environ., 15,* (8), 1407 - 1419, 1981.

Beer, J., et al., Use of ^{10}Be in polar ice to trace the 11-year cycle of solar activity, *Nature, 347,* 164 - 166, 1990.

Bolin, B., Döös, B.R., Jäger, J. (Ed.), *The greenhouse effect, climatic change, and ecosystems,* 541 pp., SCOPE 29, John Wiley & sons, 1986.

Brost, R.A., J. Feichter, and M. Heimann, Three - dimensional simulation of ^{7}Be in a global climate model, *J. Geophys. Res., 96,* (D12), 22423 - 22445, 1991.

Cambray, R.S., E.M.R. Fisher, G.S. Spicer, C.G. Wallace, and T.J. Webber, Radioactive fallout in air and rain, Results to the middle of 1963, *Rep. 4392,* U.K. Atomic Energy Auth., Res. Group, Atomic Energy Res. Estab., Harwell, Berkshire, England, 1963.

Cambray, R.S., E.M.R. Fisher, G.S. Spicer, C.G. Wallace, and T.J. Webber, Radioactive fallout in air and rain, Results to the middle of 1964, *Rep. 4687,* U.K. Atomic Energy Auth., Res. Group, Atomic Energy Res. Estab., Harwell, Berkshire, England, 1964.

Cambray, R.S., E.M.R. Fisher, W.L. Brooks, A. Hughes, and G.S. Spicer, Radioactive fallout in air and rain, Results to the middle of 1965, *Rep. 4997,* U.K. Atomic Energy Auth., Res. Group, Atomic Energy Res. Estab., Harwell, Berkshire, England, 1965.

Cambray, R.S., E.M.R. Fisher, W.L. Brooks, and D.H. Peirson, Radioactive fallout in air and rain, Results to the middle of 1966, *Rep. 5260,* U.K. Atomic Energy Auth., Res. Group, Atomic Energy Res. Estab., Harwell, Berkshire, England, 1966.

Cambray, R.S., E.M.R. Fisher, W.L. Brooks, and D.H. Peirson, Radioactive fallout in air and rain, Results to the middle of 1967, *Rep. 5575,* U.K. Atomic Energy Auth., Res. Group, Atomic Energy Res. Estab., Harwell, Berkshire, England, 1967.

Chang, J.S., R.A. Brost, I.S.A. Isaksen, S. Madronich, P. Middleton, W.R. Stockwell, and C.J. Walcek, A three-dimensional eulerian acid deposition model: Physical concepts and formulation, *J. Geophys. Res., 92,* (D12), 14681 - 14700, 1987.

Commissariat a l'Energie Atomique, Synthese Mensuelle des Mesures de radioactivite effectuees dans l'environnement des sites du groupe CEA, *Rep. DPS 90/001/3,* Dep. de Prot. Sanit., France, 1990a.

Commissariat a l'Energie Atomique, Synthese Mensuelle des Mesures de radioactivite effectuees dans l'environnement des sites du groupe CEA, *Rep. DPS 90/001/4,* Dep. de Prot. Sanit., France, 1990b.

Commissariat a l'Energie Atomique, Synthese Mensuelle des Mesures de radioactivite effectuees dans l'environnement des sites du groupe CEA, *Rep. 90/001/5,* Dep. de Prot. Sanit., France, 1990c.

Dörr, H., Investigation of the gas and water budgets in the unsaturated soil layer using carbon dioxide and radon-222 (in German), Ph.D. thesis, Univ. of Heidelberg, Germany, 1984.

Dörr, H., L. Katruff, and I. Levin, Soil texture parameterization of the methane uptake in aerated soils, *Chemosphere, 26,* 697 - 713, 1993.

Ehhalt, D.H., Turnover times of 137Cs and HTO in the troposphere and removal rates of natural aerosol particles and water vapor, *J. Geophys. Res., 78,* (D30), 7076 - 7086, 1973.

Enting, I.G., and G.I. Pearman, Description of a one-dimensional carbon cycle model calibrated using techniques of constrained inversion, *Tellus, Ser. B, 39,* 459 - 476, 1987.

Feely, H.W., H. Seitz, R.J. Lagomarsino, and P.E. Biscaye, Transport and fallout of stratospheric radioactive debris, *Tellus, 18,* 316 - 328, 1966.

Feely, H.W., L. Toonkel, and R.J. Larsen, Radionuclides and trace elements in surface air, *Rep. EML-395,* Environ. Meas. Lab., U.S. Dep. of Energy, New York, 1981.

Feely, H.W., R.J. Larsen, and C.G. Sanderson, Annual report of the surface air sampling program, *Rep. EML-497,* Environ. Meas. Lab., U.S. Dep. of Energy, New York, July 1988.

Feichter, J., R.A. Brost, and M. Heimann, Three - dimensional modeling of the concentration and deposition of ^{210}Pb aerosols, *J. Geophys. Res., 96,* 22447 - 22460, 1991.

Friedlander, M.W., *Cosmic Rays: Tracking Particles From Outer Space,* 160 pp., Harvard University Press, Cambridge, Mass., 1989.

Giorgi, F., A particle dry deposition parameterization scheme for use in tracer transport models, *J. Geophys. Res., 91,* (D9), 9794 - 9806, 1986.

Giorgi, F., and W.L. Chameides, Rainout lifetimes of highly soluble aerosols and gases as inferred from simulations with a general circulation model, *J. Geophys. Res., 91,* (D13), 14367 - 14376, 1986.

Gopalakrishnan, S., C. Rangarajan, L.U. Joshi, D.K. Kapoor, and C.D. Eapen, *Measurements on Airborne and Surface Fallout Radioactivity in India,* Gov. of India, Atomic Energy Comm., Bhabha Atomic Res. Cent., Bombay, 1973.

Graustein, W.C., and K.K. Turekian, ^{210}Pb and ^{137}Cs in air and soils measure the rate and vertical profile of aerosol scavenging, *J. Geophys. Res., 91,* (D13), 14355 - 14366, 1986.

Heimann, M., The global atmospheric tracer model TM2, *Technical Report No. 10,* Deutsches Klimarechenzentrum (DKRZ), Hamburg, Germany, 1995.

Heimann, M., and J. Feichter, A comparison of three-dimensional atmospheric transport models by means of simulations of radon-222, *GLOMAC Rep. 2,* Meteorol. Inst. der Univ. Hamburg, Germany, 1990.

Heimann, M., and C.D. Keeling, A three-dimensional model of atmospheric CO_2 transport based on observed winds, 2, Model description and simulated tracer experiments, in *Aspects of Climate Variability in the Pacific and Western Americas, Geophys. Monogr. Ser.,* vol. 55, edited by D.H. Peterson, pp. 237 - 275, AGU, Washington, D. C., 1989.

Hillas, A.M., *Cosmic Rays,* 297 pp., Pergamon, New York, 1972.

Hötzl, H., G. Rosner, and R. Winkler, Correlation of ^{7}Be concentrations in surface air and precipitation with the solar cycle, *Naturwissenschaften, 78,* 215 - 217, 1991.

Holton, J.R., *An Introduction to Dynamic Meteorology,* 2nd ed., Int. *Geophys. Ser.,* vol. 23, Academic, San Diego, Calif., 1979.

Jacob, D.J., and M.J. Prather, Radon-222 as a test of convective transport in a general circulation model, *Tellus, Ser. B, 42,* 118 - 134, 1990.

Jaeger, L., Monatskarten des Niederschlags für die ganze Erde, *Ber. Deutsch. Wetterdienstes, 18* (139), 1 - 38, 1976.

Joussaume, S., Three-dimensional simulations of the atmospheric cycle of desert dust particles using a general circulation model, *J. Geophys. Res., 95,* (D2), 1909 - 1941, 1990.

Junge, C.E., and P.E. Gustafson, On the distribution of sea salt over the United States and its removal by precipitation, *Tellus, 9,* 164 - 173, 1957.

Junge, C.E., *Air Chemistry and Radioactivity,* Academic, San Diego, Calif., 1963.

Kasibhatla, P.S., H. Levy II, W.J. Moxim, and W.L. Chameides, The relative impact of stratospheric photochemical production on tropospheric NO_y levels: A model study, *J. Geophys. Res., 96,* (D10), 18631 - 18646, 1991.

Lal, D., ^{10}Be in polar ice: Data reflect changes in cosmic ray flux or polar meteorology, *Geophys. Res. Lett., 14,* (8), 785 - 788, 1987.

Lal, D., and B. Peters, Cosmic ray produced radioactivity on the Earth, *Handb. Phys., 46,* 551 - 612, 1967.

Lambert, G., G. Polian, J. Sanak, B. Ardouin, A. Buisson, A. Jegou, and J.C. Le Roulley, Cycle du radon et de ses descendants: Application à l' étude des échanges troposphère - stratosphère, *Ann. Geophys., 38,* 497 - 531, 1982.

Lambert, G., B. Ardouin, and J. Sanak, Atmospheric transport of trace elements toward antarctica, *Tellus, Ser. B, 42,* 76 - 82, 1990.

Larsen, R.J., and C.G. Sanderson, EML surface air sampling program, 1989 data, *Rep. EML-541,* Environ. Meas. Lab., U.S. Dep. of Energy, New York, 1991.

Legates, D.R., and C.J. Willmott, Mean seasonal and spatial variability in gauge-corrected, global precipitation, *Int. J. Climatol., 10,* 111 - 127, 1990.

Levy II, H., and W.J. Moxim, Simulated global distribution and deposition of reactive nitrogen emitted by fossil fuel combustion, *Tellus, Ser. B, 41,* 256 - 271, 1989.

Louis, J.F., A parametric model of vertical eddy fluxes in the atmosphere, *Boundary Layer Meteorol., 17,* 187 - 202, 1979.

Machta, L., and R.J. List, Analysis of stratospheric strontium-90 measurements, *J. Geophys. Res., 64,* (D9), 1267 - 1276, 1959.

Martell, E.A., Enhanced ion production in convective storms by transpired radon isotopes and their decay products, *J. Geophys. Res., 90,* (D4), 5909 - 5916, 1985.

Mason, B.J., *The Physics of Clouds,* Oxford University Press, New York, 1957.

Mattsson, R., Seasonal variation of short-lived radon progeny, ^{210}Pb and ^{210}Po, in ground level air in Finland, *J. Geophys. Res., 75,* 1741 - 1744, 1970.

McHargue, L.R., and P.E. Damon, The global beryllium 10 cycle, *Rev. Geophys., 29,* 141 - 158, 1991.

Peng, T.H., W.S. Broecker, G.G. Mathieu, Y.H. Li, and A.E. Bainbridge, Radon evasion rates in the atlantic and pacific oceans as determined during the Geosecs program, *J. Geophys. Res., 84,* (C5), 2471 - 2486, 1979.

Rahn, K.A., Relative importances of North America and Eurasia as sources of arctic aerosol, *Atmos. Environ., 15,* (8), 1447 - 1455, 1981.

Raisbeck, G.M., F. Yiou, M. Fruneau, J.M. Loiseaux, M. Lieuvin, and J.C. Ravel, Cosmogenic $^{10}Be/^{7}Be$ as a probe of atmospheric transport processes, *Geophys. Res. Lett., 8,* (9), 1015 - 1018, 1981.

Rehfeld, S., Radioactive tracer deposition in an atmospheric transport model (in German), *Exam. 20,* Max-Planck-Inst. für Meteorol., Hamburg, Germany, 1994.

Reiter, E.R., Stratospheric - tropospheric exchange processes, *Rev. Geophys., 13,* (4), 459 - 474, 1975.

Russell, G.L., and J.A. Lerner, A new finite-differencing scheme for the tracer transport equation, *J. Appl. Meteorol., 20,* (12), 1483 - 1498, 1981.

Sehmel, G.A., Particle and gas dry deposition: A review, *Atmos. Environ., 14,* 983 - 1011, 1980.

Slinn, W.G.N., Formulation and a solution of the diffusion - deposition - resuspension problem, *Atmos. Environ., 10,* 763 - 768, 1976.

Slinn, W.G.N., L. Hasse, B.B. Hicks, A.W. Hogan, D. Lal, P.S. Liss, K.O. Munnich, G.A. Sehmel, and O. Vittori, Review paper: Some aspects of the transfer of atmospheric trace constituents past the air - sea - interface, *Atmos. Environ., 12,* 2055 - 2087, 1978.

Small, S.H., Wet and dry deposition of fallout materials at Kjeller, *Tellus, 12,* 308 - 314, 1959.

Staley, D.O., Strontium-90 in surface air and the stratosphere: Some interpretations of the 1963-75 data, *J. Atmos. Sci., 39,* 1571 - 1590, 1982.

Tiedtke, M., A comprehensive mass flux scheme for cumulus parameterization in large-scale models, *Mon. Weather Rev., 117,* 1779 - 1800, 1989.

Todd, J.F., G.T.F. Wong, C.R. Olsen, and I.L. Larsen, Atmospheric depositional characteristics of Beryllium-7 and Lead-210 along the southeastern Virginia coast, *J. Geophys. Res., 94,* (D8), 11106 - 11116, 1989.

Tsunogai, S., T. Kurata, T. Suzuki, and K. Yokota, Seasonal variation of atmospheric ^{210}Pb and Al in the western North Pacific region, *J. Atmos. Chem., 7,* 389 - 407, 1988.

Turekian, K.K., Y. Nozaki, and L.K. Benninger, Geochemistry of atmospheric radon and radon products, *Ann. Rev. Earth Planet. Sci., 5,* 227 - 255, 1977.

U.S. Atomic Energy Commission, Flight data and results of radiochemical analysis of filter samples collected during 1963 under project stardust, *Rep. HASL-168,* Health and Safety Lab., New York, March 15, 1966.

Warneck, P., *Chemistry of the Natural Atmosphere,* Int. Geophys. Ser., vol. 41, pp. 484 - 542, Academic, San Diego, Calif., 1988.

Wilkening, M.H., and W.E. Clements, Radon-222 from the ocean surface, *J. Geophys. Res., 80,* 3828 - 3830, 1975.

M. Heimann and S. Rehfeld, Max-Planck-Institut für Meteorologie, Bundesstraße 55, D-20146 Hamburg, Germany. (e-mail: rehfeld@dkrz.d400.de)

(Received October 11, 1994; revised March 8, 1995; accepted March 8, 1995.)